M.TECH PROJECT

ENTITLED

Synthesis & characterization of silicon carbide and carbonyl iron powder based sintered magnetic abrasive

Submitted in Partial Fulfillment for the Award of the Degree of

MASTER OF TECHNOLOGY
In
PRODUCTION ENGINEERING

Submitted By

ANKIT BANSAL

(Rol l No.: 2k11 / PIE / 01)

Under the supervision of

Shri M.S. Niranjan (Assistant Professor)

DEPARTMENT OF MECHANICAL ENGINEERING,

DELHI TECHNOLOGICAL UNIVERSITY,

(FORMERLY DELHI COLLEGE OF ENGINEERING), DELHI

(Session 2011-13)

CERTIFICATE

Date:_____

This is to certify that report entitled **"Synthesis & characterization of silicon carbide and carbonyl iron powder based sintered magnetic abrasive "** by **Mr. ANKIT BANSAL,** is the requirement of the partial fulfilment for the award of Degree of **Master of Technology (M. Tech.)** in **Production Engineering** at **Delhi Technological University**. This work was completed under our supervision and guidance. He has completed his work with utmost sincerity and diligence. The work embodied in this project has not been submitted for the award of any other degree to the best of my knowledge.

(Supervisor)   **(Co- Supervisor)**

MR. M.S. NIRANJAN   **Dr. QASIM MURTAZA**

(ASSISTANT PROFESSOR)   **(ASSOCIATE PROFESSOR)**

Department Of Mechanical Engineering,

Delhi Technological University,

(Formerly Delhi College Of Engineering), Delhi

SESSION: 2011-13

ACKNOWLEDGEMENT

CONTENTS

ii

iii

iv

LIST OF FIGURES

LIST OF TABLE

Abbreviation

PM	Powder Metallurgy
MMC	Metal matrix composite
VOL	Volume
SiC	Silicon carbide
CIP	Carbonyl iron powder
LPS	Liquid Phase Sintering
SEM	Scan electron microscope
BHN	Brinell hardness number
D	Diameter
VHN	Vickers hardness number
Kgf	kilogram force
KHN	Knoop hardness number
mm	Millimetre
MA	Magnetic abrasive
XRD	X-ray diffraction
UTM	Universal Testing Machine
VSM	Vibrating Sample Magnetometer
N	Newton
CRH	Constant rate heating
M	Meter
In	Inch
Å	Angstrom
ʎ	Wavelength

ABSTRACT

The magnetic field assisted surface finishing process needs a sintered magnetic abrasive powder. This Sintered magnetic abrasive is a mixture of SiC abrasive and ferromagnetic particle which is carbonyl iron powder. The SiC based sintered magnetic abrasives have been developed in sintering furnace.

This work is carried out using silicon carbide and carbonyl iron powder in the ratio of 20 percent by volume and rest is rheological fluid containing heavy paraffin oil and grease in the ratio of 80 and 20 percent by weight respectively. The powder is first blended mechanically in the ball mill to get the homogeneous mixture. This mixed powder is used to make pellets of 6g each by using hydraulic press at different loads of 5, 7 and 9 tones. Each pellet is kept holded for 15 minutes to achieve uniform compaction. The holding time plays an important role as there is no binder and additive used.

The green pellets are now sintered in the tubular furnace. The sintering cycle is prepared in such a way that the gases and impurity escapes below the re-crystallization temperature. The maximum temperature is kept constant for three hours to sinter the pellets properly. Solid and liquid sintering are done at 1000 and 1545 degree celcius respectively in the presence of argon environment and cooling is also done in argon atmosphere upto room temperature. Argon is a inert gas which prevent oxidation during sintering process.

Mechanical properties such as compressive strength, microstructure and microhardness has been done on sintered sample. The variation & behaviour shown by the material has been plotted on the graph. The sintered pellets are then crushed for two hours in the ball mill to get the required size of the particle. Characterization of sintered magnetic abrasives has been done using SEM, EDS, XRD and VSM to study the morphology, chemical composition, crystallography and magnetic properties. The results has been compared with the unbonded magnetic abrasives.

Keywords : Powder metallurgy, Sintering, Magnetic abrasive, Silicon carbide, carbonyl iron, SEM, XRD, VSM.

CHAPTER 1

1.1 INTRODUCTION

The engineering fraternity has always been on the lookout for wonder-materials which would fit the bills for all types of service conditions. It stem from the need to make progressive discoveries made by scientists, affordable. This affordability quotient has persuaded many researchers to develop such materials which would satisfy various hitherto unexplored conditions.

In today's world almost all generic materials have been tried for various uses and their limitations have been met. But the never ending quest of civilization requires that materials qualify for harsher environments. This unavoidable situation demands that new materials be created from various combinations of other compatible materials. It is to be noted here that this method is not new, it has been with mankind since ages. In every part of the world, various materials have been combined to achieve some intended properties, albeit each case differs from the others, i.e. one can create new materials with unique properties, which can be tailor-made and are different from their base ingredients. This concept holds true for a genre of materials called Composite materials where in, various types of matrices may be combined with reinforcements which contribute to the enhancement of the properties. Neither the matrices nor the reinforcements taken alone can stand up to the requirement, but the composite may be able to do so. This alteration in properties can be controlled by many ways, viz. controlling the matrix and reinforcement quality, their proportion or the fabrication route. This flexibility in manufacturing allows one to develop composites with varying properties in a precisely controlled fashion.

It is the superiority of properties that has triggered the penetration of composite materials into all fields of manufacturing. Metal Matrix Composites (MMCs) have emerged as a class of materials suitable for structural, aerospace, automotive, electronic, thermal and wear applications owing to their advantages over the conventional monoliths. They score over in terms of specific modulus, specific strength, high temperature stability, controlled coefficient of thermal expansion, wear resistance, chemical inertness,

etc. But the down side is populated by inferior toughness and high cost of fabrication in comparison with Polymer Matrix Composites (PMCs). But MMCs supersede in terms of higher transverse strength and stiffness, shear strength and high temperature capabilities. The physical properties that attract are no moisture absorption, non-flammability, high electrical and thermal conductivities and resistance to most radiations.

1.2 Metal Matrix Composite:

The term composite means- a solid material that results when two or more different substances, each with its own characteristics, are combined to create a new substance whose properties are superior to those of the original components for any specific application. The term composite more specifically refers to a structural material within which a reinforcement material (such as silicon carbide) is embedded and the engineering definition would also go alongside- A material system composed of a mixture or combination of two or more constituents that differ in form or material composition and are essentially insoluble in each other. In principle, composites can be fabricated out of any combination of two or more materials metallic, organic, or inorganic; but the constituent forms are more restricted. The matrix is the body constituent, serving to enclose the composite and give it a bulk form. Major structural constituents are fibers, particulates, laminates or layers, flakes and fillers. They determine the internal structure of the composite. Usually, they are the additive phase when two or more materials are interspersed, there is always a contiguous region. Simply this may be the common boundary of the two phases concerned, in which case it is called an interface. A composite having a single interface is feasibly fabricated when the matrix and the reinforcement are perfectly compatible. On the other end, there may an altogether separate phase present between the matrix phase and the reinforcement phase. This intermediate phase is called an inter-phase. In case there is an inter-phase present, there are two interfaces, one defining the boundary between the matrix and the inter-phase, and the other between the inter-phase and the reinforcement. The strength of the composite in such a case is dependent upon the strength of the weakest of the two interfaces. There are

certain advantages of having a preferred inter-phase. Such a composite with an inter-phase is fabricated if the matrix and reinforcement are not chemically compatible or if the weldability of the pair is very poor. Such a composite is materialized, by introducing a third material that has good bonding properties, individually with the matrix and the reinforcement, which would not be possible otherwise. More or less, the strength of a composite is a function of the strength of its interface between the matrix and the reinforcement. The failure of a functional composite is essentially a result of the failure of the interface. Hence the strengthening mechanism is the most dominant parameter in successful fabrication of a high strength composite. Composites differ by their matrix type, reinforcement type, size and form, composition, temper state, etc. With such a big window available for fabricating a composite from different constituent materials, it is not uncommon to experiment with materials with vividly different properties. There are three broadly classified groups of composites: Polymer Matrix Composite, Metal Matrix Composite and Ceramic Matrix Composite.

The sustained interest to develop engineering materials which could cope with the raised performance standards, resulted in emergence of a newer class of materials, called Metal Matrix Composites (MMCs). They constitute a family of customizable materials with customizable critical property relationships. Such materials are known for their exceptional high modulus, stiffness, wear resistance, fatigue life, strength-to-weight ratios and thermal expansion etc. With these enhancements in properties, they pose for strong candidature for replacing conventional structural materials. But what makes them stand apart is the ability to customize their properties to suit the service requirement. Such advantages have made this group of materials a nice pick for use in weight-sensitive and stiffness-critical components in transportation systems. MMCs can be described as a group of materials in which a continuous metallic phase (matrix) is combined with one or more reinforcement phases. The aim of such a composite material is to enhance the suitability of the end product by selectively enhancing the complimentary properties, and masking the detrimental properties of the matrix and the reinforcement. While fabricating the MMC, a solid material results when two or more substances are physically (not

chemically) combined to create a new material whose properties are superior to those of the original substances for a specific application.

1.3 Powder Metallurgy Process: Powder metallurgy (PM) is a metal

working process for forming precision metal components from metal powders. The metal powder is first pressed into product shape at room temperature. This is followed by heating (sintering)that causes the powder particles to fuse together without melting.

```
                          ┌──────────┐
                          │  Metal   │
                          │ powder   │
                          └──────────┘
                                │
  ┌───────────┐         ┌──────────────┐         ┌───────────┐
  │ Lubricants│────────▶│   Blending   │◀────────│ Additives │
  └───────────┘         └──────────────┘         └───────────┘
```

	Cold compaction			Hot consolidation		
Loose powder	Die Compaction	Cold isostatic processing	other methods Rolling Extrusion Explosive compaction	Hot Pressing	Hot isostatic Pressing	Extrusion pseudo static

```
                    ┌──────────────┐
                    │  Sintering   │
                    └──────────────┘

                          ┌──────────────┐
                          │ Hot forging  │
                          └──────────────┘

              ┌────────────────────────┐
              │  Secondary treatments  │
              └────────────────────────┘

  ┌──────────────────────────────────────────────────┐
  │               Finished PM parts                   │
  └──────────────────────────────────────────────────┘
```
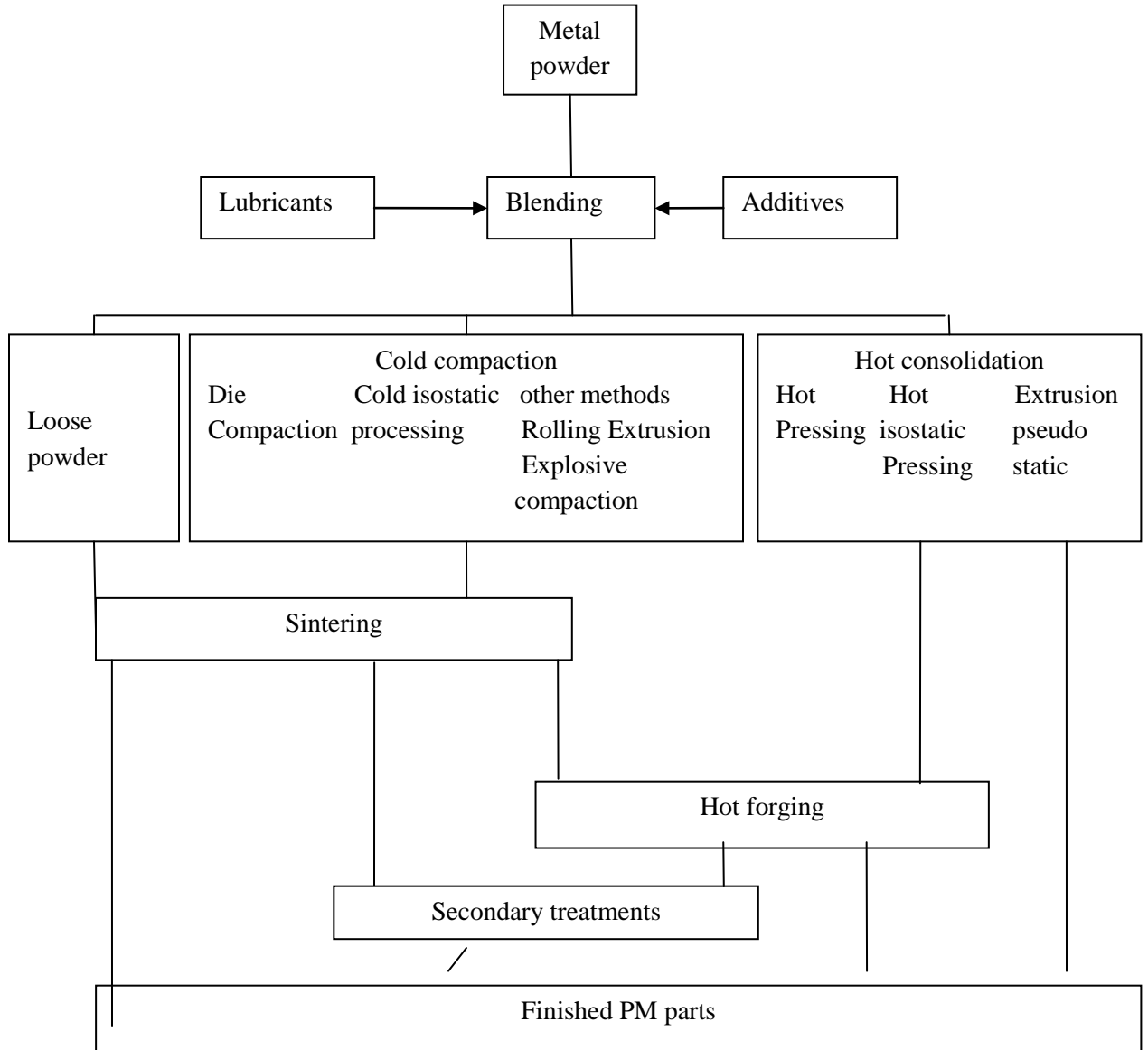
Fig 1.1 : Basic steps of powder metallurgy

The matrix may be a pure metal or any alloy suitable for the intended application. The reinforcement may be any other material in the form of particulates, whiskers, fibers, platelets etc. The most common reinforcements are ceramics and metals having nominal size in the range of 0.1 to 100 micrometers. But in fact, just about anything suitable for the application may be utilized as a potential reinforcement. Even though at times, the matrix and the reinforcement both can be metallic in nature, MMCs are not fabricated by conventional alloying methods suitable for metals; since, such a process would mar the essence of a composite. In alloys the phases are not chemically and physically distinct. But in a composite, such phases are intentionally kept distinct, to exploit the properties of the constituents to the fullest. The reinforcing phase is the nominal constituent of a composite. It is the principal load bearing component in the system. Hence the reinforcements with better mechanical properties than the matrix materials are chosen while designing a composite. The matrix is responsible for holding the load-carrying reinforcement together and retaining the bulk shape of the composite. It also shares some portion of the total load which is transferred to the reinforcement via the interface or vice versa. It is the effectiveness of the interface that decides how much load is transferred to and from the matrix. In MMCs a high degree of interaction between the matrix and the reinforcement is inherent. The resulting strength is a direct function of effectiveness of the interface between the matrix and the reinforcement. The character of the interface depends upon the chemical and mechanical compatibility of the two phases involved. The chemical incompatibility constraint can be overcome either by opting for a low-temperature processing route or by selecting stable constituents. The thermal-mechanical incompatibility problem is sorted out by employing a ductile matrix that accommodates the strain generated by the thermal alterations. Also it helps to select a pair of matrix and reinforcement having matching coefficient of thermal expansion. However when it is chemically or thermo-mechanically not feasible to fabricate a composite from a pair of constituents, an intermediate phase which is compatible with the matrix and the reinforcement may be introduced in between the two that masks the incompatibility of the original pair. This interphase prevents the chemical reaction between the matrix and the reinforcement and/or aids the matrix in accommodating the strain generated due to

any incongruous strain build-up. A soft precipitate-free layer around the reinforcing particulates limit the propagation of the crack generated at their surface by effectively reducing the stress value gradually, thereby increasing the ultimate strength. Metal matrix composites have been under constant development since the days of the World War-II. They were intended to be used in the aircrafts as structural materials. After the war ceased, no longer the purpose was the war, rather MMCs found interest in civilian uses. Today the composites are extensively used in all aspects of life, be it food packaging, medical implants, military armors, automotive applications, space applications or just about anything else. This deep penetration of MMCs in a wide spectrum of application can be attributed to the previously mentioned advantages associated with them. However, MMCs are not without some drawbacks either. Their inadequate fracture toughness and damage tolerance, poor ductility, size limitations, inhomogenity of properties, isotropy of properties stand as hindrance to their usability front. Continuous research works are underway to overcome these limitations and explore new possibilities.

2.1 Silicon Carbide An Abrasive:

Silicon Carbide is the only chemical compound of carbon and silicon. It was originally produced by a high temperature electro-chemical reaction of sand and carbon. Silicon carbide is an excellent abrasive and has been produced and made into grinding wheels and other abrasive products for over one hundred years. Today the material has been developed into a high quality technical grade ceramic with very good mechanical properties. It is used in abrasives, refractories, ceramics, and numerous high-performance applications. The material can also be made an electrical conductor and has applications in resistance heating, flame igniters and electronic components. Structural and wear applications are constantly developing.

2.2 Mechanical And Chemical Properties :

Silicon carbide is a very hard substance with a Young's modulus of 424 GPa. It is chemically inert and reacts poorly (if at all) with any known material at room temperature. The only known efficient etch at moderate temperatures is molten KOH at 400–600°C. It is practically impossible to diffuse anything into SiC. Dopants need to be implanted or grown into the material. Furthermore, it lacks a liquid phase and instead sublimes at temperatures above 1,800°C. The vapor constituents during sublimation are mainly Si, Si_2C, and SiC_2 in specific ratios, depending on the temperature.
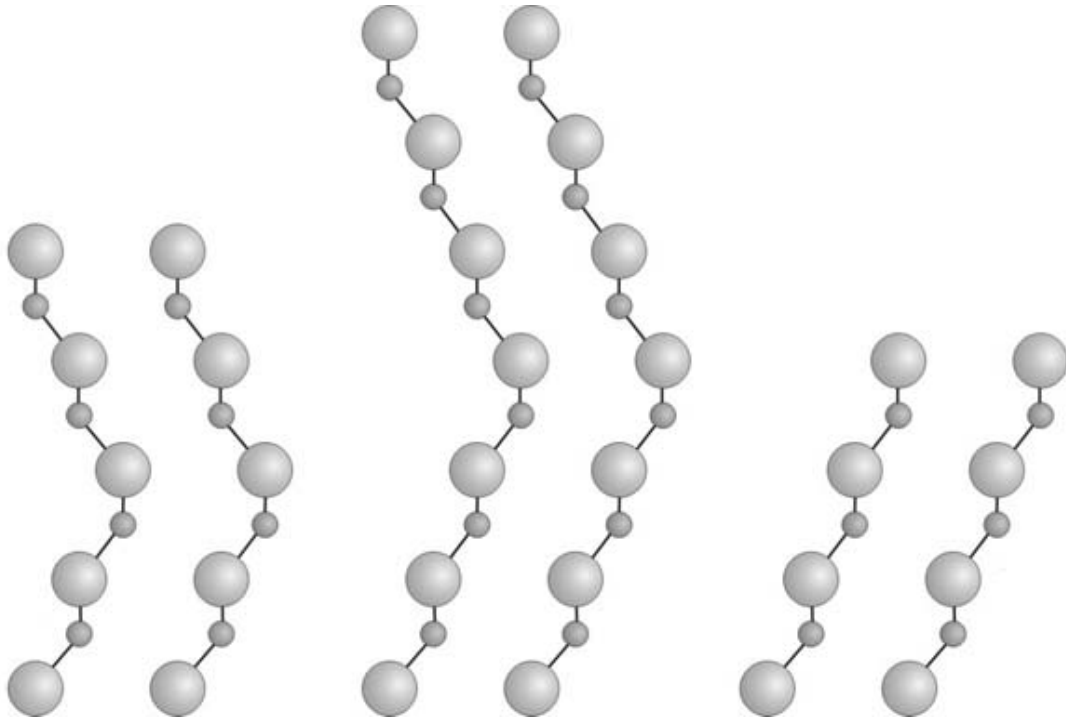
Fig 2.1 : The three most common polytypes in SiC viewed in the [1120] plane. From left to right, 4H-SiC, 6H-SiC, and 3C-SiC.

2.2.1 Key Silicon Carbide Properties :

➢ Low density

➢ High strength

➢ Low thermal expansion

➢ High thermal conductivity

➢ High hardness

➢ High elastic modulus

➢ Excellent thermal shock resistance

➢ Superior chemical inertness

2.2.2 Silicon Carbide Applications :

➢ Fixed and moving turbine components

➢ Suction box covers

➢ Seals, bearings

➢ Ball valve parts

➢ Hot gas flow liners

- ➢ Heat exchangers
- ➢ Semiconductor process equipment

2.3 Thermal Conductivity :

The second most important parameter for surface finishing applications is the material's thermal conductivity. An increase in temperature generally leads to a change in the physical properties of the rheological paste, which normally affects the machining in a negative way. It is often quoted that the thermal conductivity of SiC is higher than that of copper at room temperature. There are even claims that it is better than any metal at room temperature. The thermal conductivity of copper is 4.0 W/(cm-K). That of silver is 4.18 W/(cm-K). Values of the thermal conductivity as high as 5 W/(cm-K) have been measured by Slack on highly perfect Lely platelets. More detailed studies have been made where the thermal conductivity in the different crystal directions have been determined for SiC. As can be seen, there is a dependence on the purity of the crystal as well as on the crystal direction. At the time of this study, the material was not of the high quality we see today, and more sophisticated techniques have been developed to measure thermal conductivity. Thus, as higher-quality material has been grown, values close to the theoretical values have been measured using the laser flash technique. High-purity semi-insulating (SI) SiC material has the highest reported thermal conductivity with a value of 4.9 W/(cm-K). Lower values are measured for the doped crystals but they are all above 4 W/(cm-K) at room temperature.

2.4 General Silicon Carbide Information:

Silicon carbide is composed of tetrahedra of carbon and silicon atoms with strong bonds in the crystal lattice. This produces a very hard and strong material. Silicon carbide is not attacked by any acids or alkalis or molten salts up to 800°C. In air, SiC forms a protective silicon oxide coating at 1200°C and is able to be used up to 1600°C. The high thermal conductivity coupled with low thermal expansion and high strength give this material exceptional thermal shock resistant qualities. Silicon carbide ceramics with little or no grain boundary impurities maintain their strength to very high temperatures, approaching 1600°C with no strength loss. Chemical purity, resistance to chemical attack

at temperature, and strength retention at high temperatures has made this material very popular as wafer tray supports and paddles in semiconductor furnaces. The electrical conduction of the material has lead to its use in resistance heating elements for electric furnaces, and as a key component in thermistors (temperature variable resistors) and in varistors (voltage variable resistors).

Silicon Carbide Properties			
Mechanical	SI/Metric (Imperial)	SI/Metric	(Imperial)
Density	gm/cc (lb/ft^3)	3.1	(193.5)
Porosity	% (%)	0	(0)
Color	—	Black	—
Flexural Strength	MPa (lb/in^{2}x10^3)	550	(80)
Elastic Modulus	GPa (lb/in^{2}x10^6)	410	(59.5)
Shear Modulus	GPa (lb/in^{2}x10^6)	—	—
Bulk Modulus	GPa (lb/in^{2}x10^6)	—	—
Poisson's Ratio	—	0.14	(0.14)
Compressive Strength	MPa (lb/in^{2}x10^3)	3900	(566)
Hardness	Kg/mm^2	2800	—
Fracture Toughness K$_{IC}$	MPa•m$^{1/2}$	4.6	—
Maximum Use Temperature (no load)	°C (°F)	1650	(3000)

Table 2.1 : Properties of silicon carbide

2.5 Carbonyl Iron Powder (CIP):

CIP is produced by thermal decomposition of iron pentacarbonyl $Fe(Co)_5$, which is previously distilled to high purity. In the course of the decomposition process, spherical iron layers form on a nucleus, thereby developing a shell structure. The decomposition conditions determine the main properties, including the particle size distribution of the intermediate products. The individual CIP grades are gained from these by a number of fi nishing processes like milling (desagglomeration of secondary particles), classifying (tailoring of particle size distribution), mixing and coating.

Fig 2.2: Carbonyl Iron Powder in the pure form

2.6 Properties :

1. Its exceptional fi neness and spherical morphology leads to excellent compaction and sintering properties. These properties are exploited in diamond Tool Production, Metal Injection Molding, and conventional Powder Metallurgy.

2. Its specifi c catalytic activity is the key to the synthesis of high quality industrial diamonds.

3. Its outstanding magnetization behavior is relevant for applications such as Inductive electronic Components, Magnetorheological Fluids.

4. Its unique micro structure makes CIP an excellent absorber of microwave frequencies, enabling technologies from eMI shielding to radar absorption.

5. Its unparalleled purity and consistent high quality are the main reasons to choose for various purposes.

2.7 Applications :

1. Inductive electronic components.
2. Diamond tools
3. Milling classifying hydrogen Annealing coating
4. Microwave and radar Absorption
5. Metal injection molding and Powder Metallurgy

2.8 Hard Grade CIP: These grades are produced from the primary decomposition

products without further chemical processing.

2.8.1 Typical properties of hard grades:

• Onion skin structure

• Mechanically hard

• Fe content up to 97.8 %

• Other elements (typically): C max. 1.0 %, N max. 0.9 %, O max. 0.5 %

2.9 Soft Grade CIP: These grades are produced by annealing of hard grades under hydrogen. In this process the onion skin structure is lost, and the content of N, C, and O is reduced.

2.9.1 Typical properties of soft grades:

• Polycrystalline structure

• Mechanically soft

• Excellent compaction properties

• Fe content up to 99.8 %

• Low C, n, and o content

3.1 Literature Review :

Biswas,K. et al. (2001) : In this paper SiC ceramics incorporating sintering additives from the system $AlN–Y_2O_3$ and having variable α-SiC/β-SiC, AlN/Y_2O_3 ratios and additive contents were gas-pressure sintered to theoretical density. Post-sintering heat treatments were performed in order to induce phase transformations from β-SiC to α-SiC and anisotropic grain growth, leading to platelet-strengthened microstructures. The indentation fracture toughness of the platelet materials reached values in excess of 6MPa after annealing at 1950° C. Four-point bending strengths were measured at room temperature and at high temperatures, and were correlated with micro-structural data obtained by scanning electron microscopy and X-ray powder diffraction. Both the kinetics of the phase transformation/platelet formation and the strength retention at high temperature were found to exhibit maxima as a function of the AlN/Y_2O_3 ratio in the sintering additive. Fully dense SiC ceramics were obtained by LPS with $AlN–Y_2O_3$ additives.

While pressureless sintering in nitrogen atmosphere is effective for the complete densification of a wide range of compositions, sintering in a N_2 overpressure of 0.2–10MPa proved advantageous in view of micro-structural control. The materials obtained were fine-grained and homogeneous and have a good potential for microstructure design by the in situ growth of α-SiC platelets. The phase transformation from β-SiC to α-SiC, the anisotropic grain growth, and the evolution of high fracture toughness were all strongly correlated. Materials with 60 mol% AlN in the sintering additive exhibit the fastest kinetics. The maximum in fracture toughness depends on the amount of α-SiC seeds added to the starting powders. High-temperature strength is characterised by the occurrence of a maximum around 1200°C. The most favourable strength behaviour up to 1400°C is obtained with the 60 vol.% AlN composition. The reason for the strengthening effect at high temperatures, which is characteristic of the additive system $AlN–Y_2O_3$, is believed to be the generation of compressive stress by oxidation of intergranular oxynitride phases.

Borgstrom, H. and Nyborg, L. (2007): In this paper Borgstrom, H. and Nyborg, L. have developed classical way of persistent liquid phase sintering for various combinations of alloys of the Fe-C-P-Cu-Si system and results demonstrate the capabilities of reaching near full density for mixtures of powder of sizes commonly used for traditional uniaxial die pressing. An approach is explored for a high-vanadium alloy and the results show how almost full density with appropriate microstructure can be reached from pressureless-shaped specimens using so-called starch consolidation. The application of persistent liquid phase sintering of compacted Fe-Si-C powder mixes has been demonstrated. The optimum sintering at 1260°C following compaction at 600 MPa leads to a ductile grey iron like microstructure with yield and tensile stresses of 260 and 360 MPa, respectively. The as-sintered microstructure is heat-treatable. Including an isothermal dwell and subsequent controlled cooling during the cooling stage of the sintering cycle led to a fine pearlitic matrix grey iron like material with yield and tensile stresses of 445 and 575 MPa.

The application of supersolidus liquid phase sintering starting from pre-alloyed gas-atomised V-rich high speed steel powder has also been demonstrated. Compacts of such powder with low (1.29 wt%) and high (2.45 wt%) C content were prepared by means of a slurry technique called starch consolidation. Only vacuum sintering was insufficient to yield good densification without carbide coarsening. Introduction of nitrogen during the sintering is decisive to gain in densification while keeping microstructure control taking benefit of the well-known effects of nitrogen in widened temperature range of sintering (sintering window) and transformation of MC into MX (carbonitrides).

Borsa, C. E. et al. (1998) : In this paper the authors have explored two eutectic additive systems, namely $MnO_2.SiO_2$ (MS) and $CaO.ZnO.SiO_2$ (CZS). The additive content in Al_2O_3/5wt% SiC nanocomposite material varied from 2 to 10 wt%. Densities of up to 99% of the theoretical value were achieved at temperatures as low as

1300°C. Characterisation of the materials by XRD, indicated the formation of secondary crys- talline phases in addition to Al_2O_3 and SiC. SEM and TEM analysis showed the presence of a residual glassy phase in the grain boundaries, and an increase in the average grain size when compared to nano-composites processed without LPS additives.

This work shows that liquid phase sintering (LPS) can be used to prepare dense Al_2O_3/SiC nano- composites, at temperature as low as 1300°C. For the additive systems investigated, the best densification results occurred for additions of $MnO_2.SiO_2$. This agreed with SEM analysis of the liquid/solid interactions which showed that this system was more reactive and less viscous than $CaO.ZnO.SiO_2$ in the presence of alumina. Parallel to the improvement in densification, LPS of the nanocomposites caused some microstructural changes when compared to nano composites prepared without LPS, i.e. (i) grain growth of the alumina matrix grains, (ii) formation of residual crystalline and glassy phases, (iii) formation of elongated, platelet and abnormal grains and (iv) a heterogeneous distribution of the nano-sized SiC particles.

Ermer, E.B. et al. (2001) : The purpose of this work was to examine microstructural and structural changes in the sintered silicon carbide caused by an addition of boron andror carbon. Scanning electron microscopy, X-ray diffraction and infrared vibration spectroscopy were used to analyse these changes. The obtained results indicate that the role of sintering activators consists in modifying the grain boundary properties. The influence of boron and excess of carbon on the efficiency of SiC sintering can be explained by assuming independent roles of both elements: modification of the grain boundary properties by boron and formation of inclusions restraining the grain growth by carbon.

Gomez, E. et al. (2003) : In this paper Liquid phase sintering of SiC has been studied using different sintering aids with and without the application of pressure during sintering. After Pressureless sintering the densification behaviour of the SiC-based powder mixtures was observed to be markedly dependent not only on the type and

amount of sintering aids used, but also on the crystal structure of the SiC powder. In contrast, hipping leads to high densities in all cases, independently of the chemical composition of the mixture and the type of SiC powder used. When carbon was added to these compositions, fully dense materials were still obtained.

However, a pronounced grain growth was observed. Compositions containing additions of SiO_2 and Y_2O_3 did not show any densification after pressureless sintering, due to the high viscosity and extensive volatilisation of the liquids formed at the sintering temperature. On the other hand, fully dense specimens obtained after hiping contained crystalline intergranular phases, which turned to a vitreous structure, as Al_2O_3 was included as a third component. It was observed that pressureless sintering of SiC based ceramics in the presence of a liquid phase leads to fully dense materials provided that the liquid formed at the sintering temperature has adequate characteristics, as those formed by sintering aids like alumina and yttria.

Additionally, the liquids formed by these sintering aids solidify as crystalline intergranular phases forming the yttrium aluminium garnet (YAG). It must be pointed out that adding SiO_2 to the powder mixture has a negative effect on the densification behaviour of silicon carbide based ceramics. For all compositions of the powder mixtures and basic SiC powders studied in the present work hipping was revealed to be an effective means to produce fully dense silicon carbide based ceramics by an LPS mechanism. Also, crystalline intergranular phases were observed to be formed in all systems, however, additions of alumina as a third component in the yttria– silica system tend to lower atom mobility thus leading to the formation of glassy phases. Finally, carbon was revealed as an important sintering aid for this type of ceramics, promoting sintering by reducing the viscosity of the liquid and through the reduction of SiO2, thus improving wetting. In contrast, carbon encourages surface transport mechanisms, thus causing grain growth of the 4H hexagonal polytype at the highest temperatures.

Li, G. et al. (1997) : In this paper the authors observed the sintering process can be improved if the compact is sintered in a partial liquid phase. It is found that for sintering of metal matrix composites, because of the existence of reinforcement, the

viscosity of the liquid is very low. The volume fraction of liquid phase can be increased in comparison with the sintering of the matrix materials. The amount of extra liquid phase can be assumed by combining two extreme cases: firstly, the particulates are agglomerated together. Since SiC particulates cannot be deformed, the amount of the liquid phase required is equivalent to the amount needed to fill a block of loose particulates. That is, if a volume V_r of particulates is agglomerated, it will occupy a space of volume V_s. The difference between V_s and V_r is the amount of liquid phase needed in LPS. In the second case, the reinforcement particulates are homogeneously distributed, such as phase required.

Hence, the amount of liquid phase required for liquid phase sintering is a function of the size and the distribution of the particulates. Several examples of application are also presented in the present paper. The results of the model lead to suggestions for optimal selection of sintering temperature, particle size, and others. The extra liquid phase during liquid phase sintering can be predicted using the present model where sintering temperatures can be calculated. It is found that the smaller the reinforcement particulates, the more extra liquid phase is required due to presence of large surface area. Because of the reinforcement during liquid phase sintering of metal matrix composites, sintering temperatures have to be increased. It was experimentally found that the maximum liquid phase sintering temperature for Al 4.5%Cu 15%SiC metal matrix composite can be increased to about 1.63% in comparison with its matrix material. By some simplifications in the model, the relationship between the amount of liquid phase, particulate size, cluster size and degree of distribution of reinforcements can be understood.

Magnani, G. et al. (2004) : In this paper high density pressureless sintered silicon carbide bodies with yttria and alumina as sintering aids were obtained without sintering bed (LPSSC-NB). Sintering behaviour of this material was studied between 1850° C and 1950°C and it was compared to the liquid phase sintered SiC material obtained using sintering bed (LPSSC-B). Sintered density was 97% of the theoretical density (T.D.) at 1875°C. Mechanical properties like fracture toughness, hardness, flexural strength were determined and compared to other SiC-based materials.

In this manner we were able to demonstrate that silicon carbide could successfully be sintered by means of liquid phase mechanism also without sintering bed. This fact opens liquid phase sintered silicon carbide to a wide range of industrial application. The authors demonstrated that silicon carbide can be pressureless sintered using yttria and alumina as sintering aids and without sintering bed. YAM was detected as grain boundary phase instead of YAG due to the higher weight loss. Nevertheless, sintered density reached the value of 97 T.D.% at 1875°C. Furthermore, this material exhibits high fracture toughness and high oxidation resistance up to 1400°C that makes it potentially promising for a wide range of applications also at high temperature.

Olevsky, E. A. (1997) : Theoretical concepts of sintering were originally based upon ideas of the discrete nature of particulate media. However, the actual sintering kinetics of particulate bodies are determined not only by the properties of the particles themselves and the nature of their local interaction with each other, but also by macroscopic factors. Among them are externally applied forces, kinematic constraints *(*e.g. adhesion of the sample's end face and furnace surface*)*, and inhomogeneity of properties in the volume under investigation *(*e.g. inhomogeneity of initial density distribution created during preliminary forming operations*)*.

Insufficient treatment of the questions enumerated above was one of the basic reasons hindering the use of sintering theory. A promising approach is connected with the use of continuum mechanics, which has been successfully applied to the analysis of compaction of porous bodies. This approach is based upon the theories of plastic and nonlinear-viscous deformation of porous bodies. Similar ideas have recently been embodied in a continuum theory of sintering. The main results of the application of this theory for the solution of certain technological problems of sintering are introduced including their thermo–mechanical aspects.

Rahimian, M. et al. (2009) : The aim of this paper was to investigate the effect of alumina particle size, sintering temperature and sintering time on the properties of Al–Al$_2$O$_3$ composite. The average particle size of alumina was 25μm. Sintering

temperature and time were in the range of 500–600°C for 30–90 min. A correlation was established between the microstructure and mechanical properties. The investigated properties include density, hardness, microstructure, yield strength, compressive strength and elongation to fracture. It was concluded that as the particle size of alumina is reduced, the density is increased followed by a fall in density.

In addition, at low particle size, the hardness and yield strength and compressive strength and elongation to fracture were higher, compared to coarse particles size of alumina. The variations in properties of Al–Al_2O_3 composite are dependent on both sintering temperature and time. Prolonged sintering times had an adverse effect on the strength of the composite. Result show the relative density of Al–Al_2O_3 composite was higher in samples containing fine particle sizes. The highest relative density of 99.95% was observed in specimens sintered at 600°C. The grain size of samples having fine Al_2O_3 particles is smaller and increasing the sintering time to 90min leads to grain coarsening. The highest hardness was 76HB in specimens containing average particle size of 3μm sintered at 600 °C for 45 min. Further increase in sintering time to 90min results in a reduction in hardness to 59 HB .The finer the particle size of alumina, the greater the compressive strength and elongation. The highest strength was 318MPa, for the composite containing an average particle size of 3μm and sintered at 600 °C for 45 min. Further increase in sintering time has an adverse effect on the strength. Extended sintering times and also the use of fine alumina in Al–Al_2O_3 composite results in higher elongations. Maximum elongation was observed to be 61.8% in samples containing the average particle size of 3μm.

Rodriguez, M.C. et al. (2005) : The influence that the atmosphere (N2 or Ar) and sintering time have on microstructure evolution in liquid-phase-sintered αSiC (LPS-α-SiC) and on its mechanical properties at high temperature was investigated. The microstructure of the samples sintered in N_2 was equiaxed with a grain size of 0.70 μm and a density of 98% of the theoretical value regardless of the sintering time. In contrast, samples sintered in Ar had an elongated-grain microstructure with a density decreasing from 99 to 95% and a grain size increasing from 0.64 to 1.61 μm as the sintering time increased from 1 to 7 h. The mechanical behaviour at 1450 °C showed the samples

sintered in nitrogen to be brittle and fail at very low strains, with a fracture stress increasing from 400 to 800MPa as the sintering time increased.

In contrast, the samples sintered in Ar were quasi-ductile with increasing strain to failure as the sintering time increased, and a fracture stress strongly linked to the form and size of the grains. These differences in the mechanical properties of the two materials are discussed in the text. During mechanical tests, a loss of intergranular phase takes place in a region, between 50 and 150 μm thick, close to the surface of the samples the effect being more important in the samples sintered in Ar. The microstructure characterization of the as-received samples showed a homogeneous distribution of the intergranular phases, and a density close to 98% of the theoretical value independently of the sintering time for samples sintered in nitrogen. For samples sintered in argon, the density decreased as the annealing time increased, being 95% for the longest annealing time. The microstructure of the samples sintered in nitrogen was unchanged with increasing sintering time, and the grains were equiaxed with an average size of 0.70μm. For the samples sintered in argon, the grain size increased from 0.64 to 1.61 μm, and the grains became ever more elongated as the sintering time increased from 1 to 7h. For the nitrogen sintered samples, the flow stress increased from 350 to 750MPa and the maximum stress from 400 to 800MPa as the annealing time was prolonged from 1 to 7 h. This was a consequence of the incorporation of nitrogen into the intergranular phase. For the argon sintered samples, the flow stress remained between 350 and 400MPa and the failure stress between 500 and 550 MPa, almost independently of the sintering time. For the longest sintering time, the flow stress was 650MPa and the failure stress was 800MPa, due to the large elongated grains present in the microstructure.

The almost unchanged morphology of the grains after deformation and the redistribution of the intergranular phase indicated that grain boundary sliding and the squeezing of the intergranular phase constituted the mechanism controlling deformation. The absence of any accommodation process led to the creation of cavities and cracks, and their coalescence was the cause of the failure of the material. The differences in behaviour between the nitrogen and the argon sintered samples were due to the different microstructures generated in the two types of sample, and to the incorporation of nitrogen

into the intergranular phase leading to increased viscosity at high temperatures and rigidity of the glass network.

She, J.H. and Ueno, K. (1999) : In this paper submicron silicon carbide (SiC) was sintered to about 98% of its theoretical density by using alumina and yttria as sintering additives. This densification was attributed to the liquid-phase sintering of a eutectic liquid formed between Al_2O_3 and Y_2O_3 at sintering temperatures. Observation by scanning electron microscopy (SEM) revealed that SiC exhibited a uniformly distributed finegrained microstructure and a highly intergranular fracture behavior. The maximum values of strength and toughness were as high as 650 MPa and 7.5 MPam$^{1/2}$, respectively.

The improved toughness is considered to be associated mainly with the deflection of cracks along interphase boundaries, due to a weak interface, as well as with the introduction of microcracks at the interface between SiC grains and the secondary phases, due to a residual tensile stress from thermal expansion mismatch.

Van dijen, F. K. and Mayer, E. (1995) : The authors showed that the decomposition reactions during the sintering of liquid phase silicon carbide (SiC) can be described well by thermodynamics. This allows for an optimization of the sintering parameters. The use of carbon as a sintering additive, together with, for instance, yttria plus alumina, is of advantage. When C is used, SiO, will not occur in the liquid phase during sintering or in the amorphous and crystalline phases after sintering. The microstructure of sintered samples is described. There is excellent agreement between the theoretical aspects and experimental results. When sintering in Ar at 1900°C weight loss can be limited by the use of carbon as a sintering additive; very little aluminium vaporizes off. The use of carbon as a sintering additive has no negative effect on sintering rate or the microstructure of the sintered material.

It is suggested that the liquid phase is free of silica when carbon is used as a sintering additive. Similar remarks hold for the crystalline phases after cooling of the sintered material. No amorphous phases were found in the material after sintering in Ar at

1900°C with C. Owing to the absence of silica, this is to be expected. Therefore, liquid phase sintering of SIC is more similar to the sintering of AlN to the sintering of Si_3N_4. When sintering in N_2, AlN is formed and will dissolve in the SiC grains during sintering, as known from the phase diagram of SiC-AlN. Upon cooling the AlN leaves the Sic grains and precipitates at the grain boundaries. LP-SiC is an excellent material, especially when carbon is used as a sintering additive. Sintering in Ar at 1900°C is recommended. When C is used, the second phase is free of silica, crystalline and less weight loss during sintering is observed. The second phase is present at the triple points and no grain boundary or glassy phases are detected. Excellent high temperature properties are anticipated.

CHAPTER 4

4.1 Magnetic Abrasive Finishing / Abrasive Flow Machining:

A magnetic abrasive finishing process is defined as a process by which material is removed, in such a way that the surface finishing and deburring is performed with the presence of a magnetic field in the machining zone. The method was originally introduced in the Soviet Union, with further fundamental research in various countries including Japan. Nowadays, the study of the magnetic field assisted finishing processes is being conducted at industrial levels around the world. Most of the previous research work has been focused on the finishing characteristics and mechanism from a macroscopic point of view using the surface roughness profiles as the measure. However, those approaches do not adequately characterize the behavior of abrasive cutting edges acting against the surface during the removal process.
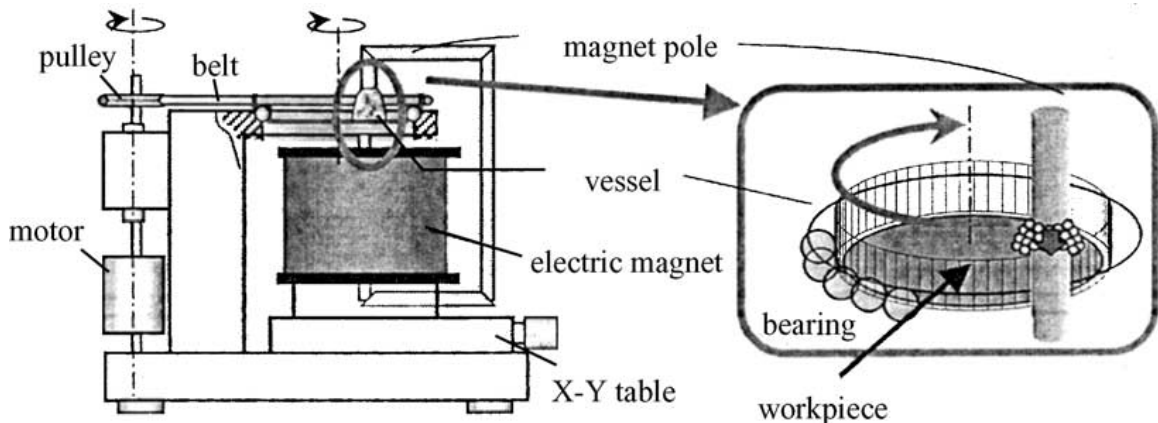
Fig 4.1 : Schematic diagram of a plenary magnetic abrasive polishing apparatus.

In order to clarify the mechanism of magnetic abrasive polishing, a planar type process for a non-magnetic material, stainless steel, was examined in the earlier research. A magnetic abrasive brush was formed between a magnetic pole and a workpiece material, in which the summation of three kinds of energy necessary for magnetization of abrasives, i.e. repulsion between bundles (Faraday effect) and line tension of outer curved bundle was considered to be minimum. A normal force that pushes the abrasives on the

brush end to be indented into the material surface is generated by the magnetic field. The magnetic abrasive brush will then be an extension of the magnetic pole. In this process, the tangential force acts to be the returning force created when the abrasive deviates from the magnetic balance point. Thus, the magnetic abrasives are expected to polish the material surface softly.
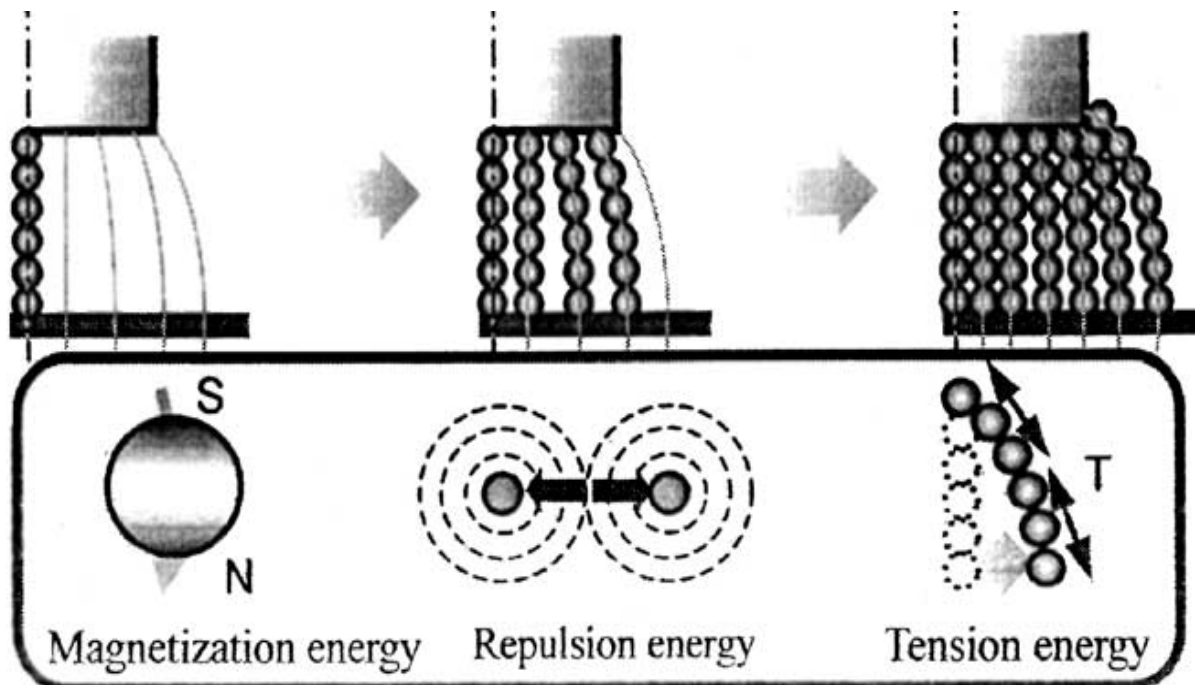
Fig 4.2 : Configuration of magnetic abrasive brushes.

4.2 Formation of magnetic abrasive brush :

The structure of the magnetic abrasive brush was certified by a method shown in Figure shown below. After forming the magnetic abrasive brush from a lower pole to an acrylic plate, which was placed instead of a workpiece, it was observed from upper side by a CCD camera. A forming mechanism of a magnetic abrasive brush can be clarified from observations made on in various abrasive volumes; mass of abrasive was varied from 0.1 to 1.0 g by 0.1 g.
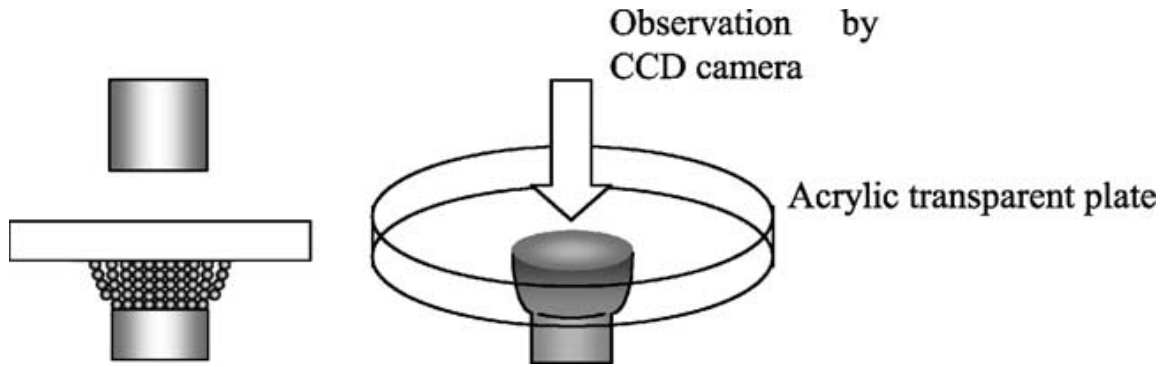
Fig 4.3 : Observation method of structures of magnetic abrasive brush.

The characteristics of the observed brush are as follows:

(i) At an abrasive small volume, the diameter of each bundle is in the order of a few hundred micrometer that are separated from each other.

(ii) With an increase of volume, the bundles get closer to other and the diameter of the bundles increase to several hundred micrometer, corresponding to several abrades.

(iii) At large abrasive volume, the maximum diameter of a bundle dose not increase but the number of bundles of several diameter increase.

These phenomena can be explained from the viewpoint of the brush forming energy. At a smaller volume of abrades, the tension energy acting on the outer side of the curved bundles is smaller than the magnetization energy:

$$dWm > dWt$$

On the other hand, when the increase of the curvature of the outmost bundle becomes too large or the separation of bundles becomes too short, the diameter of the bundle becomes large even though the magnetization energy is large:

$$dWf > dWm, dWt > dWm$$

However, the diameter of the bundle is limited because the differential factor of energy to diameter is assumed to increase abruptly. The tangential component of the tension in the outer curved bundles is directed inward and repulsion between bundles adds up in the inner side. Thus, the abrasives of the brush edge are held firm by these tangential forces. The holding force is thus strong at the inner side of the abrasive brush.
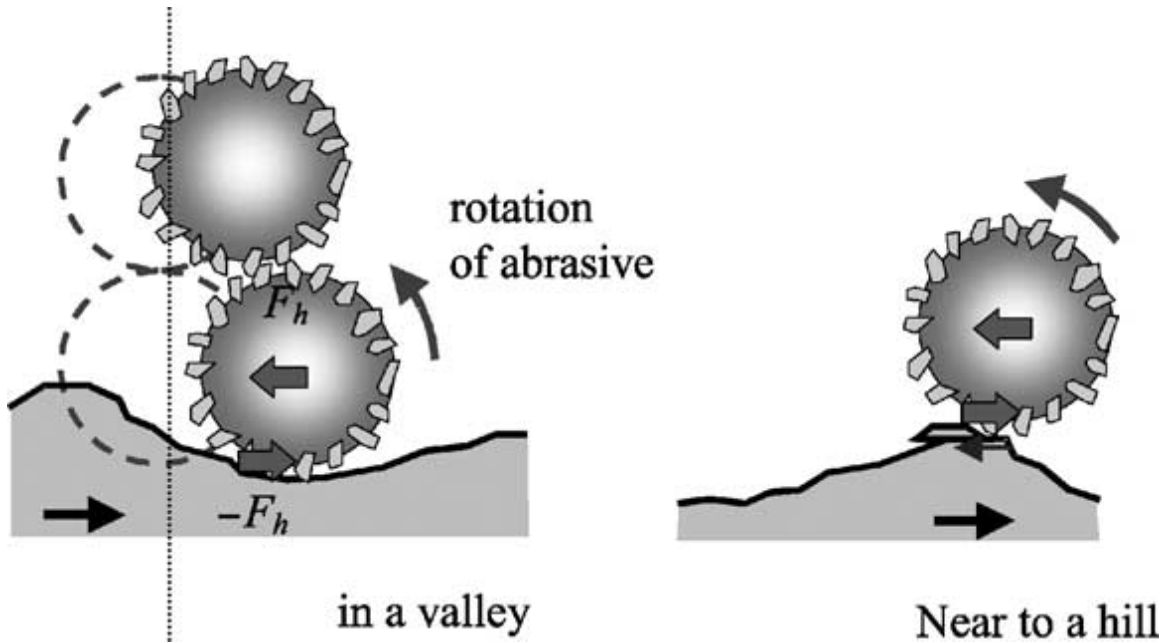
Fig 4.4 : Mechanism of magnetic abrasive polishing.

Characteristics of magnetic abrasive polishing are summed as follows:

A normal and tangential forces, acting on the magnetic abrasive at brush edge, are generated by magnetic field. Each bundle is separated from each other. By taking into account these characteristics, a polishing mechanism peculiar to this process can be explained, as shown in the above figure. At the beginning of process abrasives at the brush edge are indented into various parts of the surface. When the material moves, the abrasives repulses each other and is distanced from the balancing point and thus a return force Fh is generated. If the abrasive indenting point is near to a hill of surface roughness, material removes by Fh. On the other hand, when the abrasive stands in a valley of surface roughness it cannot cut a material. In this case, the return force Fh acts at the center of the abrasive but a reaction Fh does at the edge of indenting alumina particle. Therefore, a moment acts on the abrasive and it climbs a hill with rotating. As a volume to be removed becomes smaller at the top of the hill due to climbing and the return force Fh, growing large, exceeds the cutting resistance of the material, the abrasive cuts off the material. An abrasive after using a process in 30 min is round, and this certifies that it rotates.

5.1 Liquid Phase Sintering : Liquid phase sintering (LPS) is a process for forming high performance, multiple-phase components from powders. It involves sintering under conditions where solid grains coexist with a wetting liquid. Many variants of LPS are applied to a wide range of engineering materials. Example applications for this technology are found in automobile engine connecting rods and high-speed metal cutting inserts. Scientific advances in understanding LPS began in the 1950s. The resulting quantitative process models are now embedded in computer simulations to enable predictions of the sintered component dimensions, microstructure, and properties. However, there are remaining areas in need of research attention. Based on over 25 publications, outlines what happens when mixed powders are heated to the LPS temperature, with a focus on the densification and microstructure evolution events.

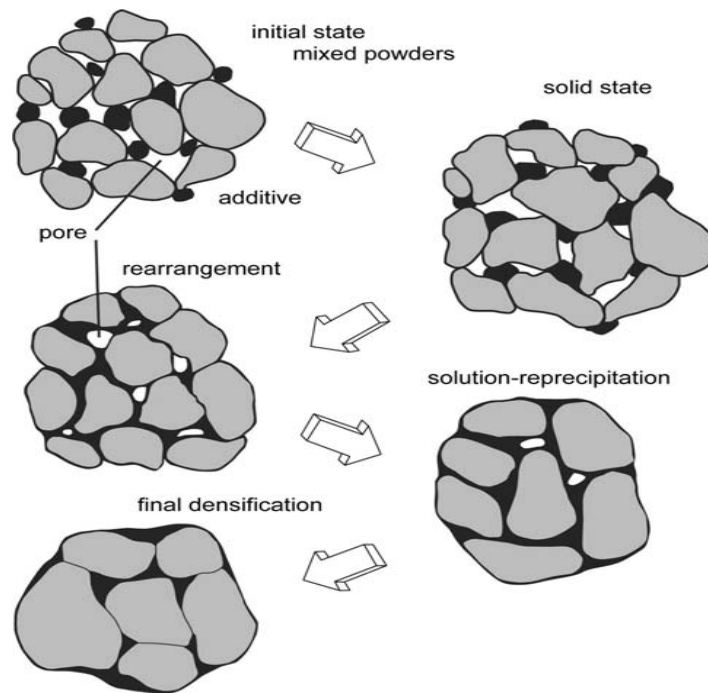**Fig 5.1 : A schematic of the microstructure changes during LPS, starting with mixed powders and pores between the particles.**

Each phase in the LPS microstructure is characterized by shape and size distributions, and variations in the degree of connection. The greatest attention is devoted to the solid grain size. Coarsening gives a steady-state morphology that changes length

scale as time progress. The structures appear similar except for the difference in magnification. The study of LPS focuses on linking composition, processing, and properties, with recent attention to improved dimensional precision. The glue between these factors is in the microstructure. A homogeneous green structure greatly improves the LPS response. The amount and placement of the liquid phase have significant impact on the sintering trajectory. Most effective is placement of the liquid phase on the interface between the solid grains. As a consequence, coated powders are an ideal starting point. Further, the identification of additives that improve wetting, accelerate diffusion, or harden the composition are linked to interfacial energy and phase relations.

5.2 Sintering cycle

5.2.1 Process variables : The most important factors involved during the sintering process are temperature ,time and furnace atmosphere. The influence of these factors on the sintering process is described below:

5.2.2 Sintering temperature: Increasing the sintering temperature greatly increases the rate and magnitude of any change in the properties occurring during the sintering. Electrical conductivity improves at very low sintering temperatures, while strength is developed after higher sintering temperatures, reaching a saturation earlier than the elongation at fracture. The strength may decrease at the highest sintering temperatures due to grain coarsening.

5.2.3 Sintering time: Although the degree of sintering increases with increasing time, the effect is small in comparison to the temperature dependence. The loss of driving force with increasing time at any temperature is difficult. An attempt should be made to achieve the desired properties of the sintered parts by shorter sintering times and corresponding higher temperatures.

5.2.4 Sintering atmosphere: The proper production, use and control of sintering atmospheres which are essential for the optimum use of the powder metallurgy process. Optimum sintering cycles have been found from literature.

5.3 High temperature tube furnace for Sintering process :

A **tube furnace** is an electric heating device used to conduct syntheses and purifications of inorganic compounds and occasionally in organic synthesis. The usual design consists of a cylindrical cavity surrounded by heating coils, which are embedded in a thermally insulating matrix. Temperature is controlled via feedback from a thermocouple. More elaborate tube furnaces have two (or more) heating zones useful for transport experiments. Some digital controllers allow RS232 interface and permit the operator to program up to 126 segments, such as ramping, soaking, sintering, and more. Also, advances in materials for heating elements, such as molybdenum disilicide offered in certain models by Vecstar, can now produce working temperatures up to 1800 °C, which facilitate more sophisticated metallurgical applications. Most commonly, the tubes are made of alumina, Pyrex or fused quartz.

Fig 5.2 : Tube furnace having facility of microprocessor temperature controller

Fig 5.3 : Tube furnace mfg by Metrex scientific instruments pvt ltd

water cooling jacket : Only require water cooling in long time running when the working temperature would be more than 900 degree.

Circulating water rate: 0.5 m^3 / hr.

Temperature control is done by PID automatic control via SCR (Silicon Controlled Rectifier) power control.

Fig 5.4: Chiller connected to the tube furnace to control the heating and cooling rate

6.1 Experimental procedure :

Wt. of the silicon carbide powder	= 3.21 g/cc X 20 cc	= 64.2 g
Wt. of the carbonyl iron powder	= 7.87 g/cc X 20 cc	= 157.4 g
Total wt. of the sample	= 64.2 + 157.4 g	= 221.6 g
Weight of each pellet to be formed	= 6 g	
Total no. of pellet to be formed	= 15	

6.2 Mixing of the powders:

To make the proper rheological paste , 20% CIP powder and 20% SiC by volume are mixed for fabricating the composite. Mixing is carried out in a lab ball mill with stainless steel jar and stainless steel balls. The powder to ball ratio was 1:1 by weight and in the crushing this ratio was 1:5 by weight. The inner diameter of the jar was 135 mm and the average diameter of the balls were 10 mm for the stainless steel ball. Referring to previous works, the speed of rotation was chosen to be 150 rpm.

6.3 Optimization of mixing time:

Mixing was carried out for a period of 30minutes and the the machine was stopped for a period of 30 minutes to cool down the vial. This stop and go sequence was repeated until 6 hours of cumulative mixing time 40.

Fig 6.1 : Set-up of ball mill having automatic timer and variable speed facility.

6.4 Compaction of the powder mix:

About 6 grams of the powder mix was taken adopting a method of coning and quartering for compaction in a cold uniaxial press in a metallic die-punch arrangement.

6.5 Cold Uniaxial pressing:

The above mentioned powder mix was pressed in the Cold uniaxial pressing machine at an incident load of 5, 7 and 9 tonne. A stainless steel die of 11.8 mm internal diameter was used for this purpose. To allow the powder to flow freely and to prevent the specimen from sticking on to the walls, stearic acid was used as a lubricant that was applied to the walls of the die and punch.

Fig 6.2 : Hydraulic jack set-up having 15 ton capacity

S. No.	Weight of the sample (g)	Load applied (ton)	Time in (minutes)	Time out (minutes)	Duration
1	6	5	10.50	11.05	15
2	6	5	11.09	11.24	15
3	6	5	11.29	11.44	15
4	6	5	11.48	12.03	15
5	6	5	12.08	12.23	15

Table 6.1 : Preparation of pellet at 5 ton load

S. No.	Weight of the sample (g)	Load applied (ton)	Time in (minutes)	Time out (minutes)	Duration
1	6	7	15.08	15.23	15
2	6	7	15.31	15.46	15
3	6	7	15.50	16.05	15
4	6	7	16.15	16.30	15
5	6	7	10.23	10.38	15

Table 6.2 : preparation of pellet at 7 ton load

S. No.	Weight of the sample (g)	Load applied (ton)	Time in (minutes)	Time out (minutes)	Duration
1	6	9	14.27	14.42	15
2	6	9	14.50	15.05	15
3	6	9	15.09	15.24	15
4	6	9	15.28	15.43	15
5	6	9	15.48	16.03	15

Table 6.3 : preparation of pellet at 9 ton load

6.6 Sintering of the green pellets:

Green pellets obtained after cold isostatic pressing were subjected to sintering in a high temperature tubular furnace. Sintering was done in the solid state only. Sintering temperature and the time of holding were varied. Previous researchers had shown that melting of the composite was occurring in a temperature range of 1000-1600 C.

A confirmatory DSC test on the specimen showed that partial melting started as early as 1000 C. With each temperature, the time of holding was varied as 1 hour, 2 hours and 3 hours. For each combination of time and temperature, different batches of samples were treated. Each batch of sample comprised of 3 specimen. Each batch was placed in the tubular furnace. The tube was sealed and evacuated to 10-4 mbar. Pure argon gas was passed through the tubular furnace for the entire duration of sintering to prevent oxidation of iron and silicon carbide. Heating rate was maintained at 6 C/minute.
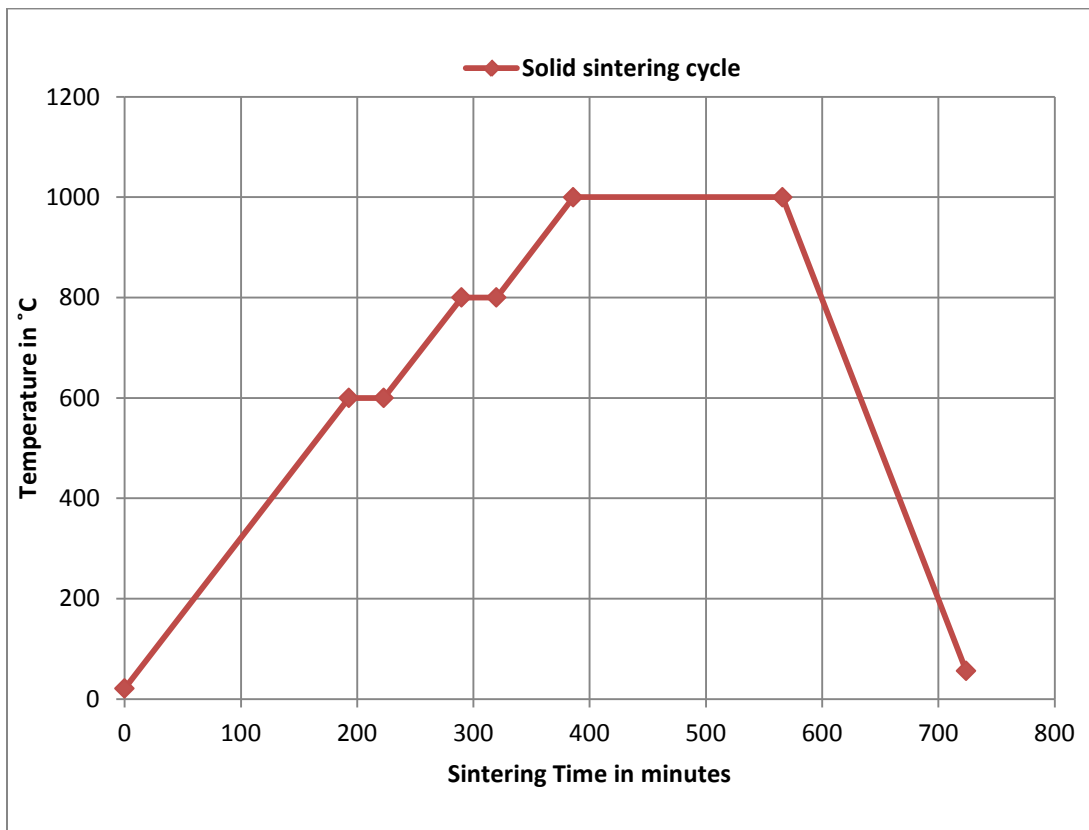
Solid phase sintering cycle for SiC+CIP
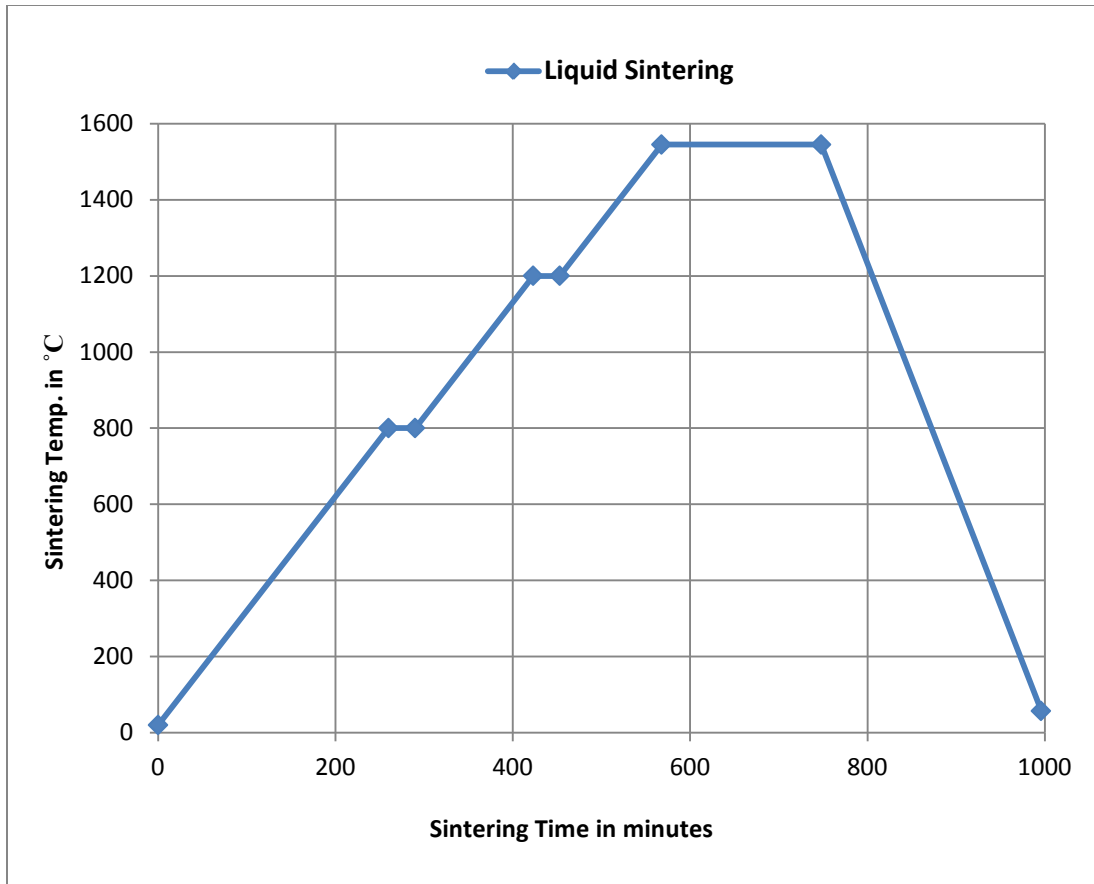
Liquid phase sintering cycle for SiC+CIP

6.7 Crushing of the sintered pellets :

After sintering the pellets are tested on universal testing machine to measure the compressive strength. The value arranged in the desired sequence clearly shows the variation of load on its strength. Simultaneously the variation of strength is observed while changing the temperature of the cycle.

The pellets are then crushed in the ball mill keeping the ratio of pellets to balls 1:25 so that powder would have required particle size. The ball mill speed should be moderate to avoid the sticking of balls to the jar wall.

7.1 Determination of the compressive strength:

Compression test was done on an Instron 4482 universal testing machine. The samples were prepared as per the ASTM E9 (extended) standard for compression test of hard metals. The cylindrical specimens were compressed at a crosshead velocity of 1mm per minute. The readings were available from a calibrated automated loadcell.

Fig 7.1 : Sintered specimen before fracture
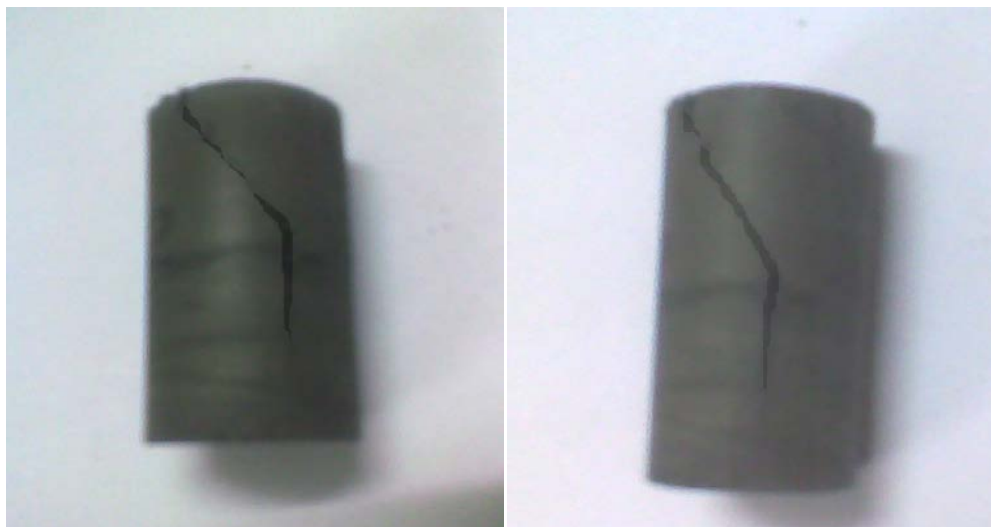
Fig 7.2 : Sintered specimen after fracture

Fig 7.3 : Universal Testing Machine set-up

S. No.	Sample type	Load applied (KN)	Cross sectional area of pellet (mm^2)	Compressive strength (N/mm^2)
1	5 ton solid	9.631	132.732	72.56
2	7 ton solid	10.220	132.732	77.00
3	9 ton solid	11.866	132.732	89.40
4	5 ton liquid	9.967	132.732	75.09
5	7 ton liquid	11.564	132.732	87.12
6	9 ton liquid	13.369	132.732	100.72

Table 7.1 : Results for the compressive strength
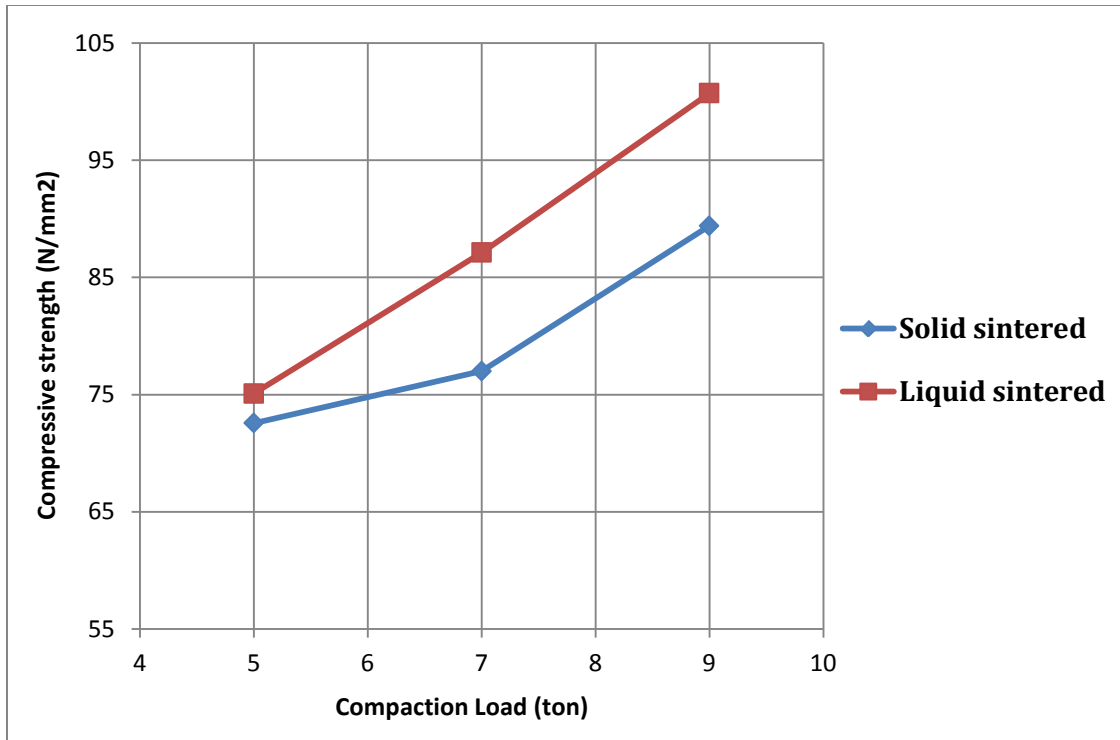
Compressive strength vs compaction load for two different sintering cycles

7.2 Density Measurement and calculation:

Bulk density increase with increase in compaction load of sintered pellets due to decrease in volume of pellets and also density of sintered pellets is higher than the green pellets as the shrinkage phenomenon occurs at elevated temperature.

❖ Theoritical density of the powder may be calculated as below relation :

Density of silicon carbide powder	=	3.21 g/cc
Density of carbonyl iron powder	=	7.81 g/cc
Mass fraction of silicon carbide	=	64.2 / 221.6
Mass fraction of carbonyl iron	=	157.4 / 221.6

$$\frac{1}{\rho} = \sum_n \left(\frac{Xi}{\rho\,i}\right) \quad where\ Xi\ is\ mass\ fraction\ of\ component\ i$$

Hence, Density of total powder mixture   =   5.51 g/cc

❖ Density measurement for the green pellet:

Weight of the each sample pellet   =   6 g

Diameter of each sample pallet   =   13 mm

Area of cross-section of the pellet   = $\frac{\pi d^2}{4}$ =   132.73 mm^2

S. No.	Compaction Load (ton)	Sintering type	Length of the pellet (mm)	Density (green sample)	Density (Sintered sample)
1	5	Solid	15.32	2.95 g/cc	3.43 g/cc
2	7	Solid	14.38	3.14 g/cc	3.52 g/cc
3	9	Solid	13.74	3.29 g/cc	3.57 g/cc
4	5	Liquid	15.38	2.94 g/cc	3.48 g/cc
5	7	Liquid	14.26	3.17 g/cc	3.56 g/cc
6	9	Liquid	13.87	3.26 g/cc	3.59 g/cc

Table 7.2 : Density variation at different load and sintering cycle
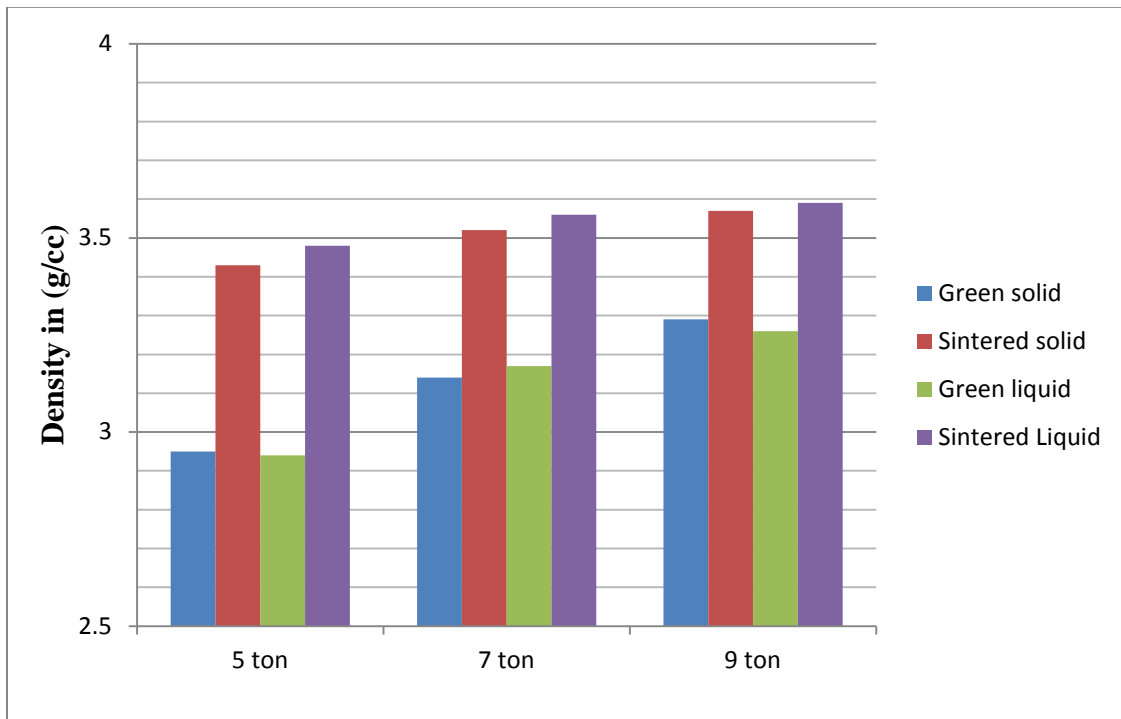
Density variation for the green and sintered sample

7.3 Micro-indentation Hardness Testing:

Micro-indentation hardness testing is a very valuable tool for the materials engineer, but it must be used with care and full understanding of potential problems. Hardness is the resistance offered by the crystal for the movement of dislocations and practically it is the resistance offered by the crystal for localized plastic deformation. The purpose of micro-indentation hardness testing is to study fine scale changes in hardness, either intentional or accidental. The technique is also commonly known as micro-hardness testing, but this term is misleading because it implies that the hardness is extremely low, which is not the case. The applied load and the resulting indent size are small relative to bulk tests, but the same hardness number is derived. Consequently, ASTM recommends the term "micro-indentation hardness testing".

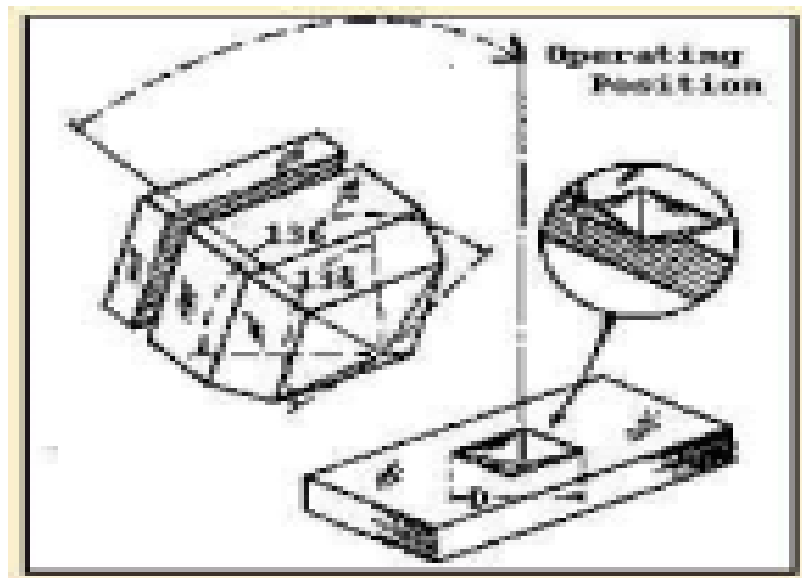**Fig 7.4 : Schematic diagram of shape of the Vickers indenter and impression.**

The ideal d / D ratio (d = impression diameter, D = ball diameter) for a spherical indenter is 0.375. If tangents are drawn to the ball at the impression edges for d / D = 0.375, they meet below the center of the impression at an angle of 136 degrees, the angle chosen for the Vickers indenter. Diamond allows the Vickers test to evaluate any material

and, furthermore, has the very important advantage of placing the hardness of all materials on one continuous scale. This is a major disadvantage of Rockwell type tests, for which 15 standard and 15 superficial scales were developed. Not one of these scales can cover the full hardness range. The HRA scale covers the broadest hardness range, but this scale is not commonly used. In the Vickers test, the load is applied smoothly, without impact, and held in place for 10 or 15 seconds. The physical quality of the indenter and the accuracy of the applied load must be controlled to get the correct results. After the load is removed, the two impression diagonals are measured, usually with a filer micrometer, to the nearest 0.1 μm, and then averaged. The Vickers hardness (HV) is calculated by: HV = 1854.4L / d^2 where the load L is in grams-force and the average diagonal d is in μm (although the hardness number units are expressed in units of kgf / mm^2 rather than the equivalent gf / μm^2).

S. No.	Sample Load in (tons)	Sintering Cycle	Microhardness at Vicker Tester	Corrosponding Microhardness at Rockwell
1	5	Solid	538	51.6
		Liquid	647	57.8
2	7	Solid	580	54.1
		Liquid	672	58.9
3	9	Solid	635	57.1
		Liquid	693	59.8

Table 7.3 : Microhardness Values corrosponding to vicker and rockwell
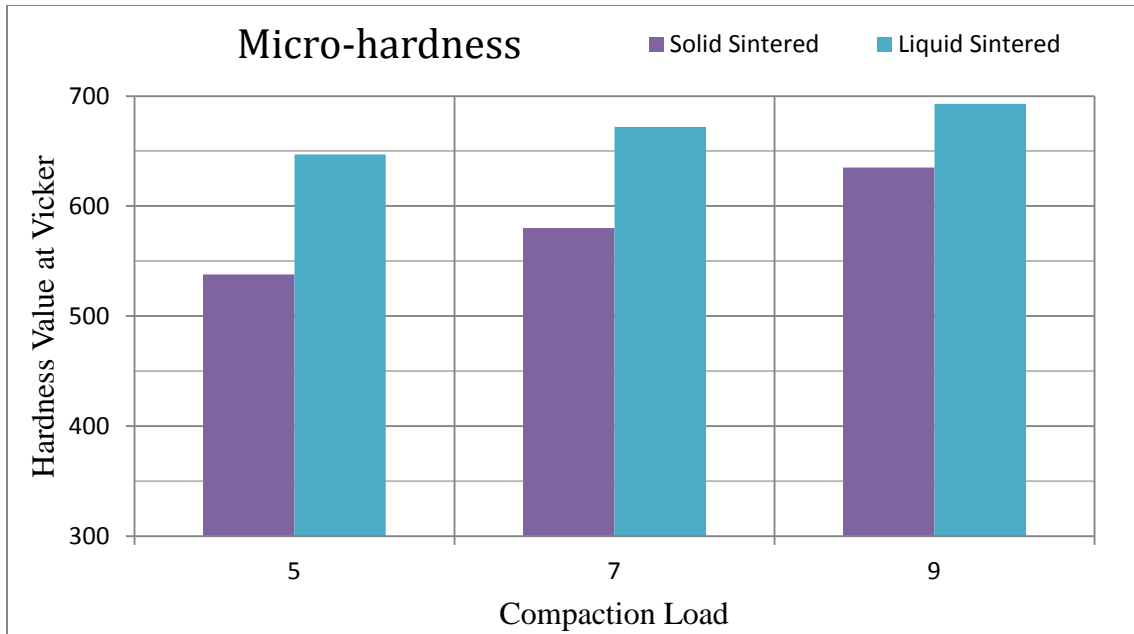
Effect of sintering temperature and compaction laod on hardness value

The original Vickers testers were developed for test loads of 1 to 120 kgf, which produce rather large indents. Recognizing the need for lower test loads, the National Physical Laboratory (U.K.) experimented with lower test loads in 1932. The first low-load Vickers tester was described by Lips and Sack in 1936. Because the shape of the Vickers indentation is geometrically similar at all test loads, the HV value is constant, within statistical precision, over a very wide test load range, as long as the test specimen is reasonably homogeneous.
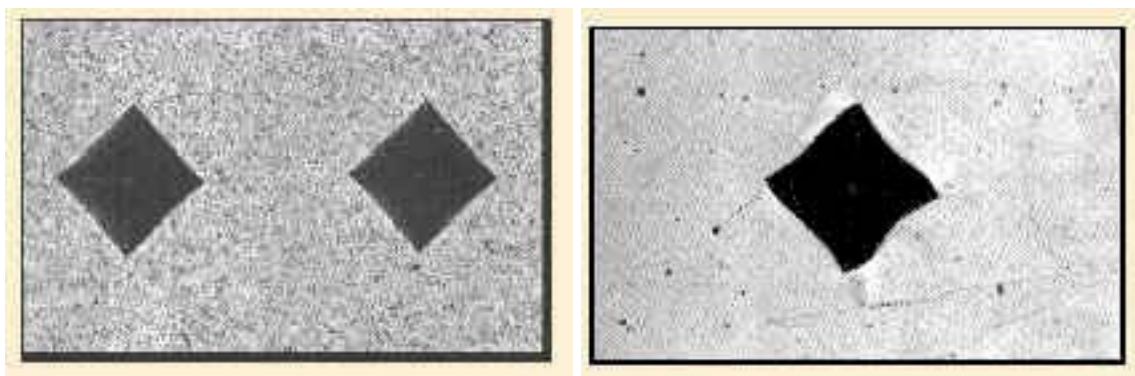

Fig 7.5 : Example of Properly formed indents and distorted Vickers indent in a specimen.

Many factors can influence the quality of micro-indentation test results so it can be classified in three main categories.

1. **Instrument Factors :** Accuracy of the applied load, Inertia effects, speed of loading, Angle of indentation, Lateral movement of the indenter or specimen, Indentation time, Indenter shape deviations, Damage to the indenter, Insufficient spacing between indents or from edges.

2. **Measurement Factors:** Calibration of the measurement system, Resolving power of the objective, Magnification, Operator bias in sizing, Inadequate image quality, Non-uniform illumination.

3. **Material Factors**: Heterogeneity in composition or microstructure, Crystallographic texture, Quality of the specimen preparation, low reflectivity or transparency.

7.4 Mechanical Polishing prior to micro-structural examination:

Polishing involves the use of abrasives, suspended in a water solution, on a cloth-covered electrically powered wheel. Standard sized aluminum oxide powders are applied for general use purposes. Following the final 600 grit fine-grinding stage, the sample MUST be washed and carefully dried before proceeding to the first polishing stage. At the polishing stages, even hard dust particles in the air which settles on the polishing cloth can cause unwanted scratching of the specimen. Careful washing of the specimen and the operator's hands must be carried out prior to each stage of polishing. Beginning with 25-micron suspended aluminum oxide particles (suspended in water) on a Nylon-cloth, the final fine-grinding surface layer resulting from the previous grinding procedure should be completely removed with a rotation rate of 150-200 rpm.

The specimen is initially held at one position on the wheel, without rotation, until most of the previous grinding marks are removed. It can be rotated slowly, counter to the wheel rotation, until only scratches from the 25- micron aluminum oxide are visible. During the initial polishing stage, moderate pressure can be applied to the specimen and the entire stage should generally take 1 or 2 minutes.

After carefully washing the specimen, proceed to the 5-micron stage where a separate polishing wheel with 5- micron particles; repeat the procedure outlined above using lighter pressure and a gradual rotating motion across the polishing cloth.

The final polishing stage with 1-micron suspended aluminum oxide particles should be carried out on a separate polishing wheel following "Careful washing of the specimen and operator's hands" at a slower speed of 100 - 150 rpm using a napped cloth. After 1 or 2 minutes a properly polished specimen should have a mirror-like surface free of scratches. During final polishing, minimal pressure should be applied and time should be kept to a minimum since the napped material will conform to the specimen shape under pressure.

The wetness of the cloth used for Final Polishing has a great influence on the end result. If the cloth is too wet the sample will show pits; if too dry, buffing and smearing will result. To determine the proper wetness, the sample should be removed from the wheel and the time required for the polishing film to dry (five to eight seconds) should be checked. A thin opaque film indicates that sufficient abrasive is present.

For precision work, Cerium Oxide is especially excellent for the final polishing of aluminum and other soft metals and alloys.

Fig 7.6 : Wet polishing and dry polishing of the sample specimen in metallurgy lab.

7.5 Etching of the specimen:

Microscopic examination of a properly polished, unetched specimen will reveal only a few structural features such as inclusions and cracks or other physical imperfections. Etching is used to highlight, and sometimes identify, micro-structural features or phases present. Even in a carefully prepared sample, a surface layer of disturbed metal, resulting from the final polishing stage, is always present and must be removed. Etchants are usually dilute acid or dilute alkalis in water, alcohol or some other solvent. Etching occurs when the acid or base is placed on the specimen surface because of the difference in rate of attack of the various phases present and their orientations. The etching process is usually accomplished by merely applying the appropriate solution to the specimen surface for several seconds to several minutes.

Nital , a Nitric Acid - Alcohol mixture, is the etchant commonly utilized with common irons and steels. Nital is dripped onto the specimen using an eye-dropper or cotton swab. Ten seconds to one minute is usually sufficient for proper etching depending on sample and nital concentration. The sample is then immediately washed under running water, rinsed with alcohol and dried in an air blast. Dry off the rinsing alcohol on the specimen with the air blast and then move on to the microscopic examination stage.
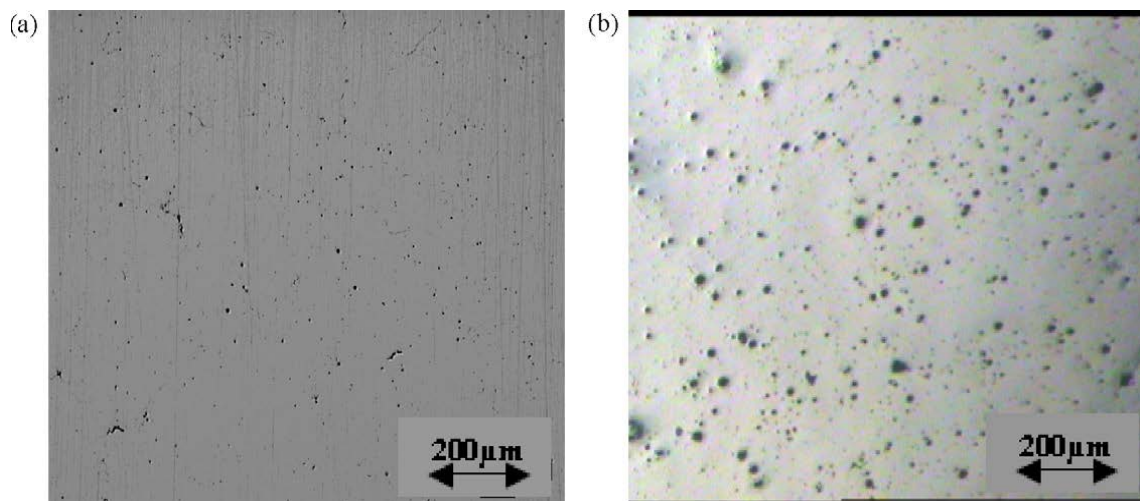
Fig 7.7 : Optical micrograph of (a) iron and (b) iron–SiC composite sintered

7.6 Scan Electron Microscope:

Scanning electron microscopy (SEM) uses a focused electron probe to extract structural and chemical information point-by-point from a region of interest in the sample. The high spatial resolution of an SEM makes it a powerful tool to characterize a wide range of specimens at the nanometer to micrometer length scales. SEM offers below stated analysis for the sample:

- Topographic imaging of materials such as fracture surfaces, nano-particles etc.
- Beam deceleration unit and cryo-sample stage for imaging beam sensitive specimens. A range of coating options is available for non-conducting samples.
- Field-free mode for imaging magnetic samples.
- Identification of elements from boron upwards using energy and wavelength dispersive X-ray analysis.
- Luminescent properties of materials.
- Electrical properties of materials.

Fig 7.8 : Outlook view of the SEM machine connected with pump and computer

7.6.1 SEM micrograph images :
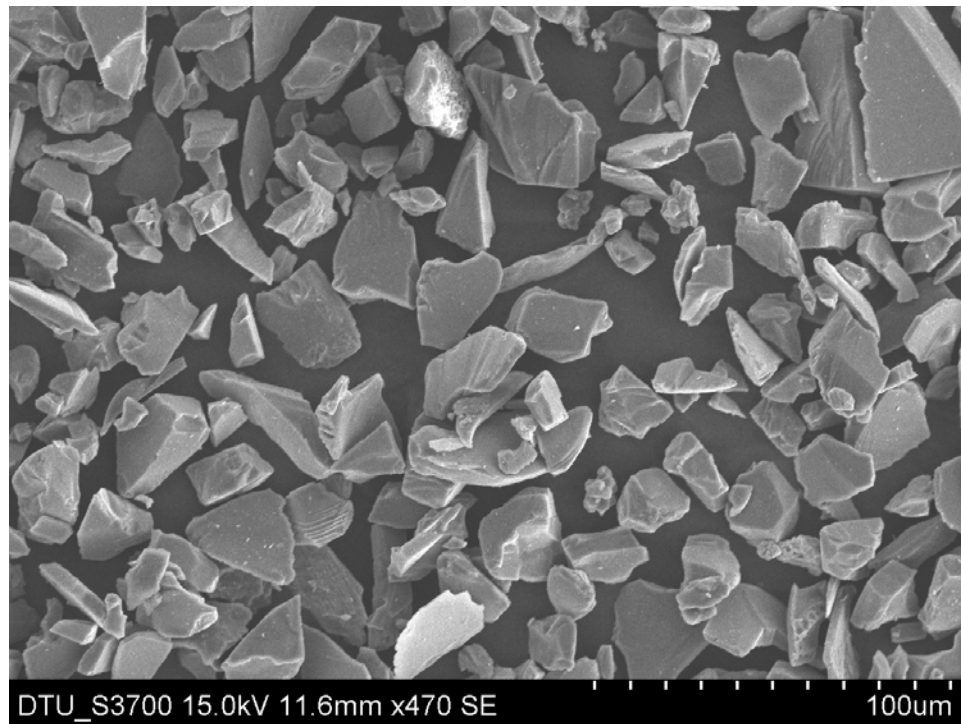
Fig 7.9 : Silicon carbide particle of 400 mesh size
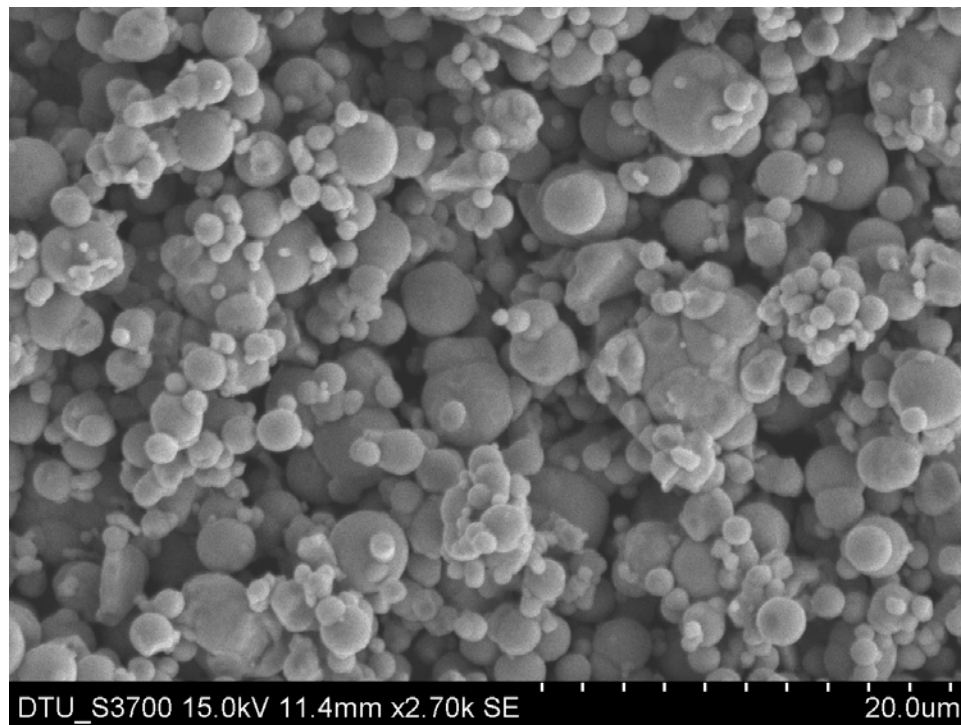
Fig 7.10 : Carbonyl iron powder of 1000-2400 mesh size
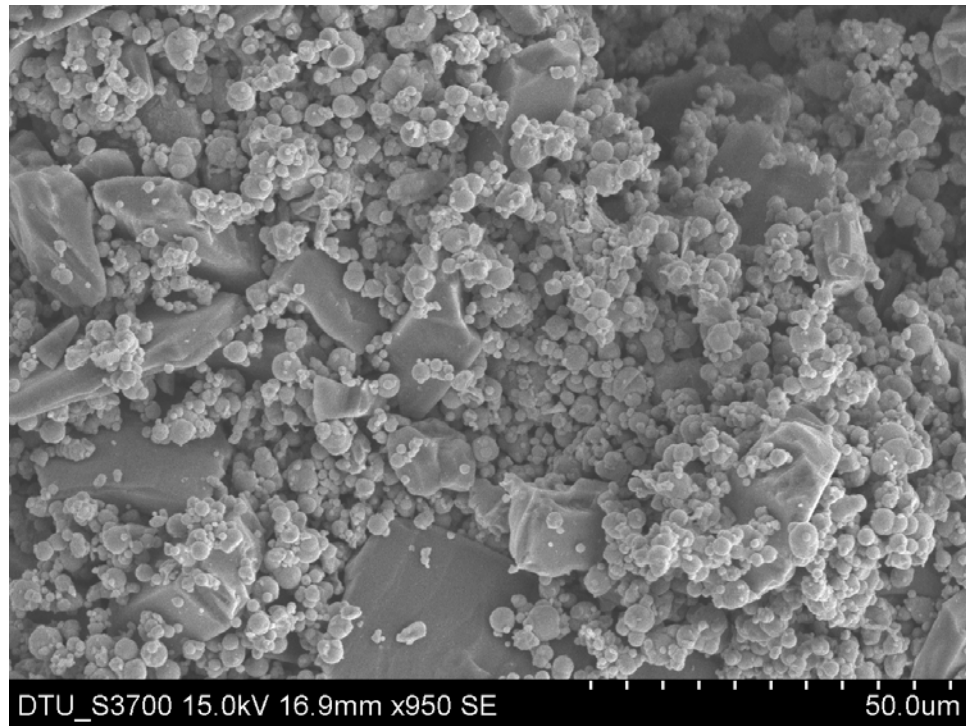
Fig 7.11 : Unbonded SiC and CIP having abrasive and magnetic properties
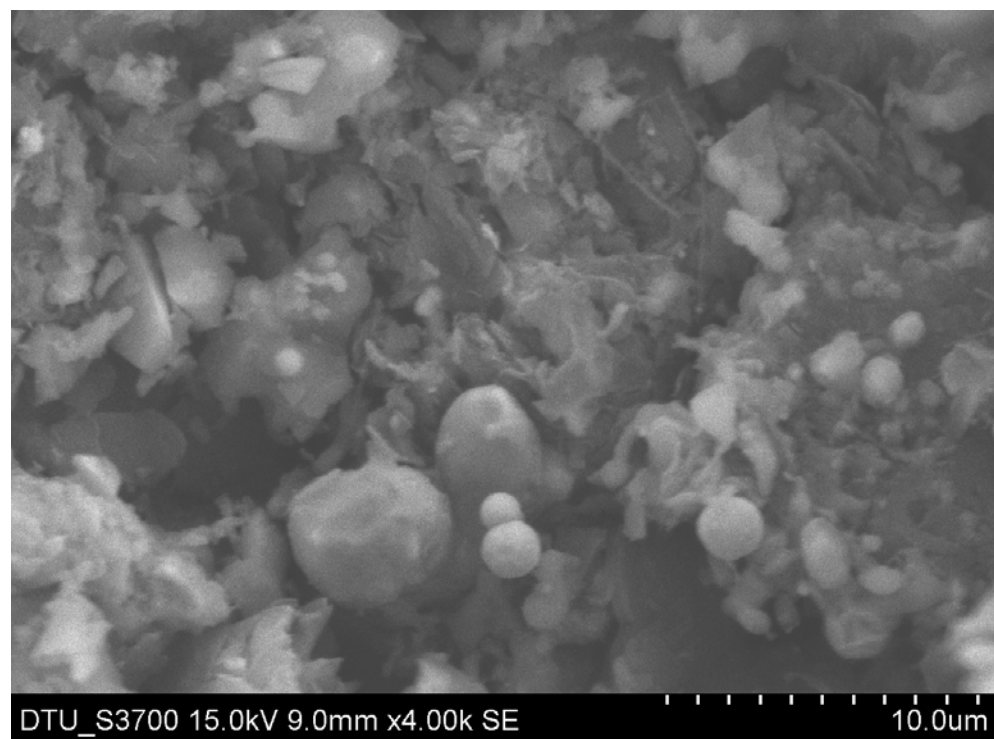
Fig 7.12 : Liquid sintered powder at 5 ton load with 4000X magnification
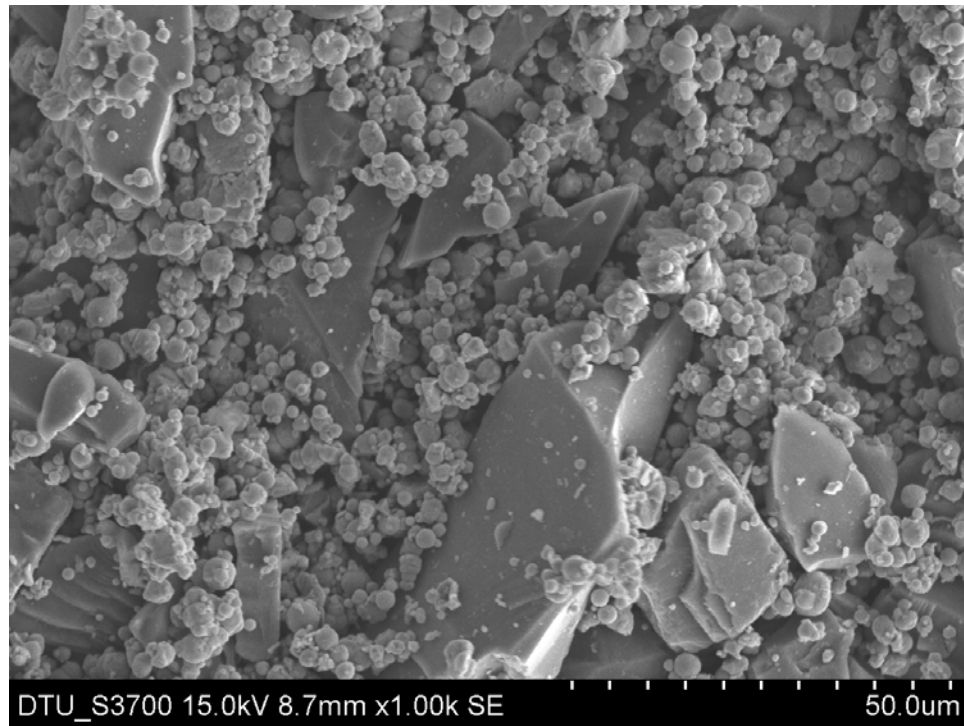
Fig 7.13 : Solid sintered powder at 5 ton load compaction with 1000X magnification
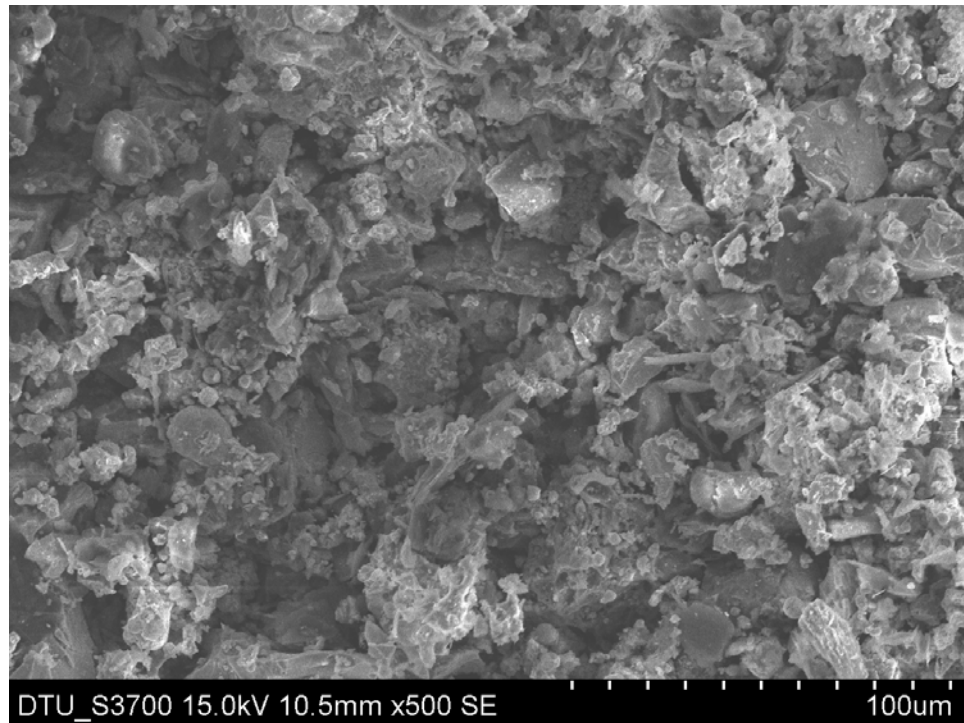
Fig 7.14 : Liquid sintered powder at 7 ton load with 500X magnification
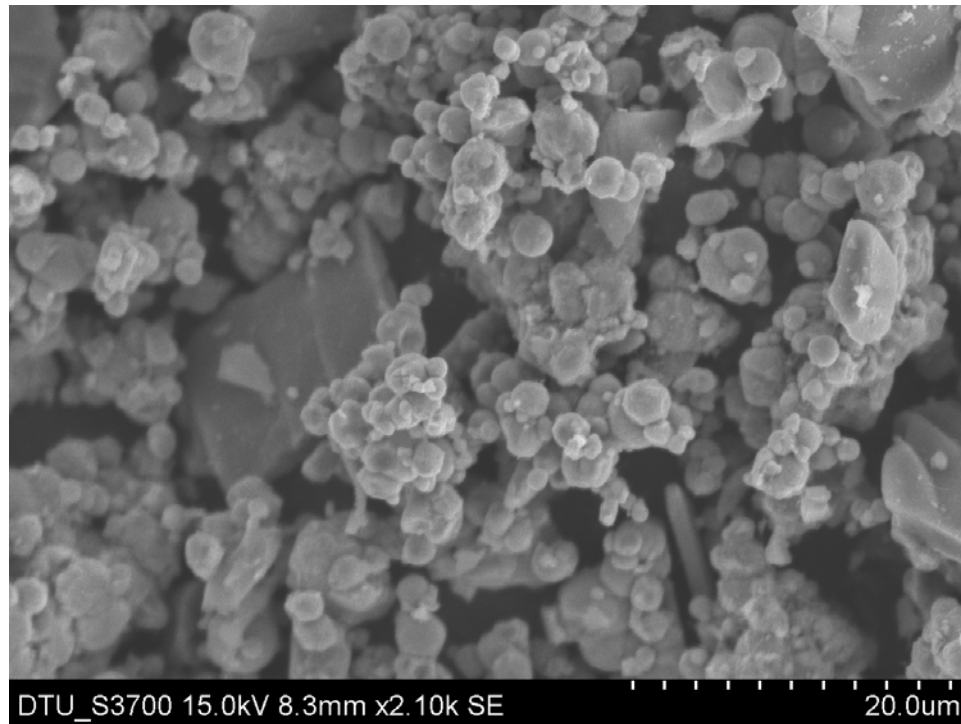
Fig 7.15 : Solid sintered powder at 7 ton load compaction with 2100X magnification
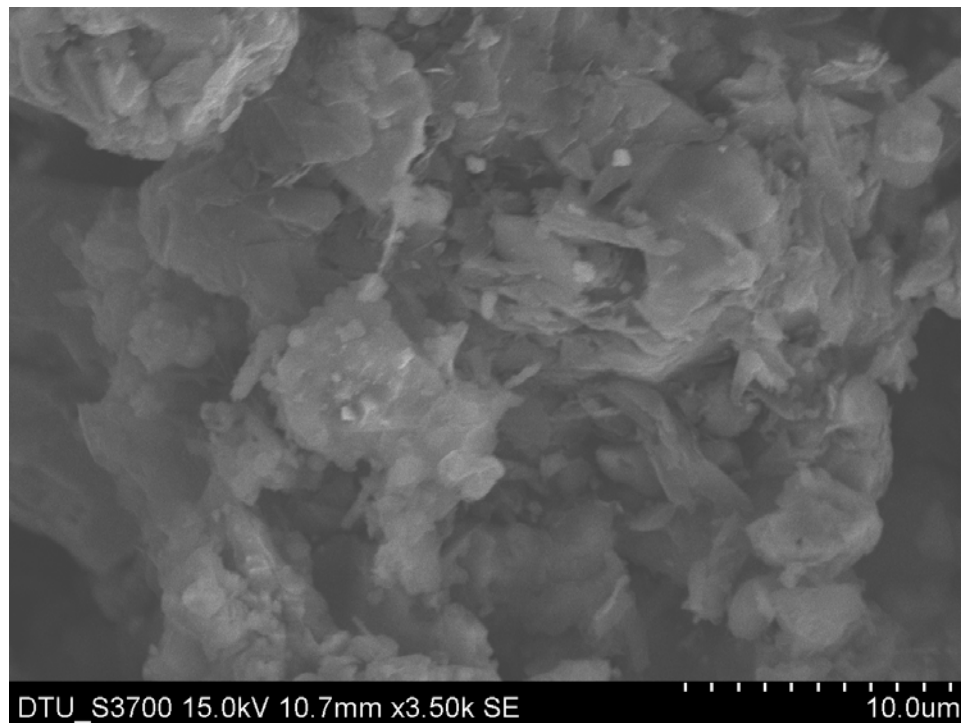
Fig 7.16 : Liquid sintered powder at 9 ton load with 3500X magnification
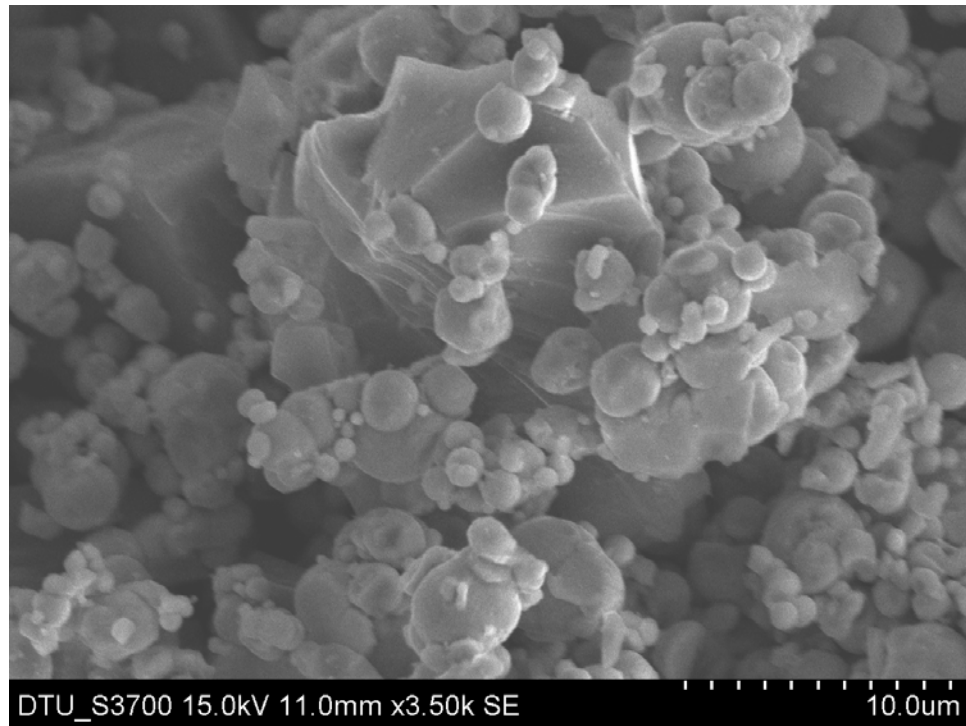
Fig 7.17 : Solid sintered powder at 9 ton load compaction with 3500X magnification
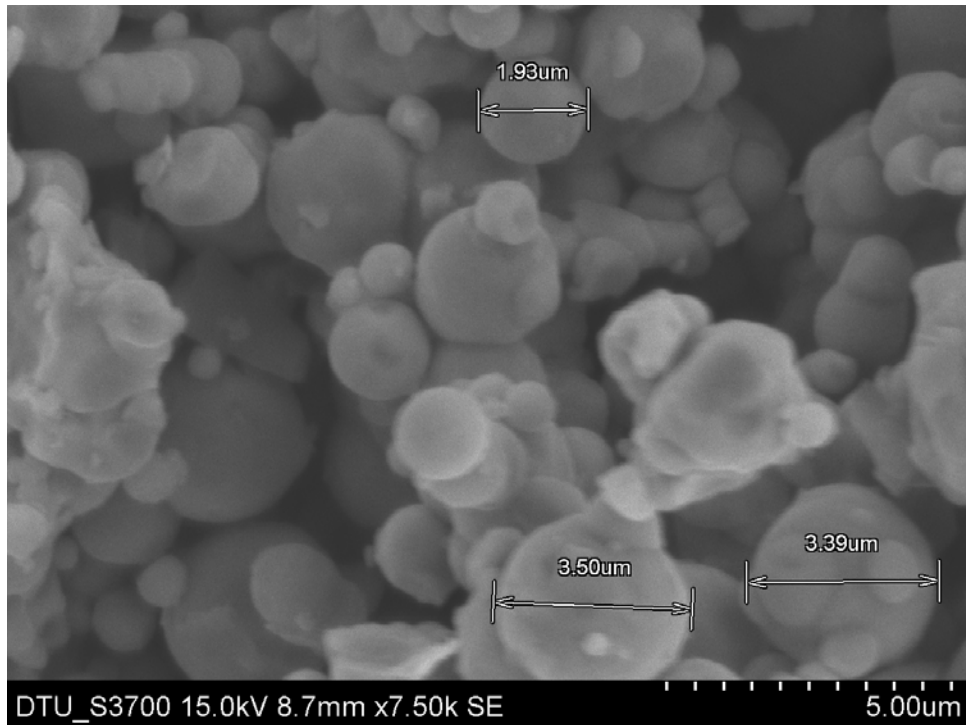
Fig 7.18 : Image showing the Average / Mean particle size taken at 7500X

7.7 Energy Dispersive Spectroscopy (EDS):
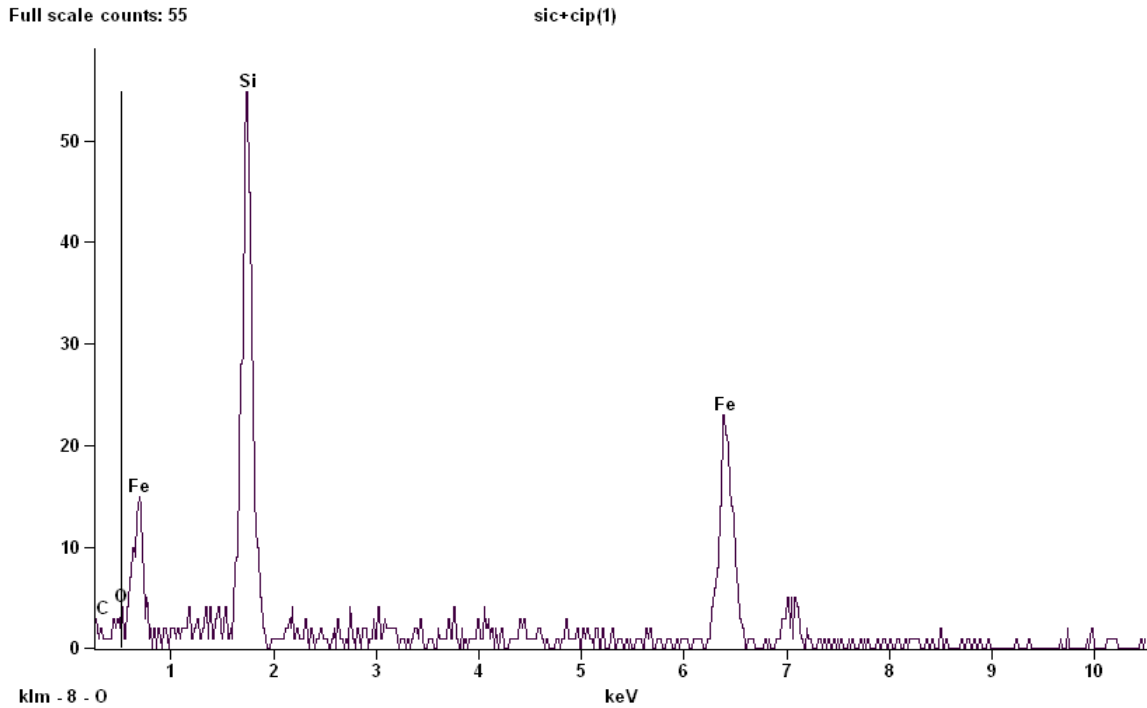
Graph showing the approximate content in the mixture before sintering

Acc.Voltage: 15.0 kV Take Off Angle: 50.5 deg.

Element Line	Net Counts	Int. Cps/nA	Weight %	Weight % Error	Atom %	Atom % Error	Formula	Standard Name
C K	0	0.000	1.69	---	0.00	+/- 0.00		C
O K	2	0.000	1.42	+/- 0.85	0.58	+/- 2.33		O
Si K	564	0.000	26.86	+/- 1.43	42.03	+/- 2.24		Si
Si L	0	0.000	---	---	---	---		
Fe K	327	0.000	70.03	+/- 6.91	57.39	+/- 5.44		Fe
Fe L	159	0.000	---	---	---	---		
Total			100.00		100.00			

Table 7.4 : Quantitative Results for unbonded mixture before sintering
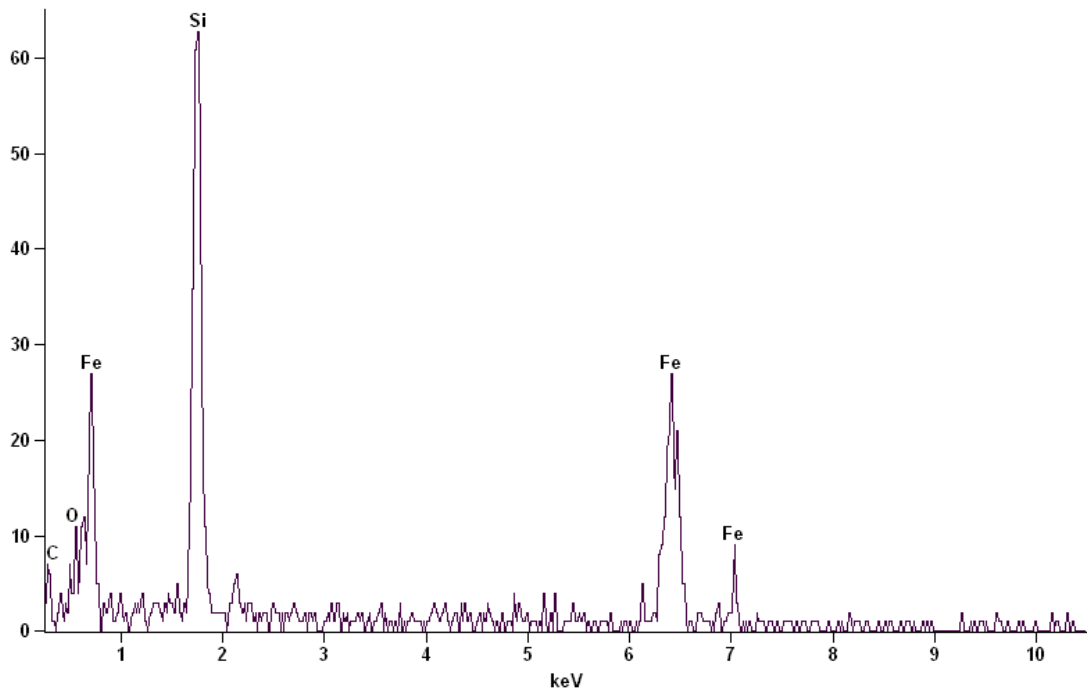
Graph showing the approximate content in the mixture after solid sintering

Element Line	Net Counts	Int. Cps/nA	Weight %	Weight % Error	Atom %	Atom % Error	Formula	Standard Name
C K	21	0.000	2.45	+/- 0.70	8.25	+/- 2.36	C	
O K	23	0.000	1.74	+/- 0.68	4.40	+/- 1.72	O	
Si K	579	0.000	25.94	+/- 0.86	35.96	+/- 1.24	Si	
Si L	0	0.000	---	---	---	---		
Fe K	323	0.000	69.88	+/- 7.02	51.39	+/- 5.09	Fe	
Fe L	207	0.000	---	---	---	---		
Total			100.00		100.00			

Table 7.5 : Quantitative Results for solid sintered sample
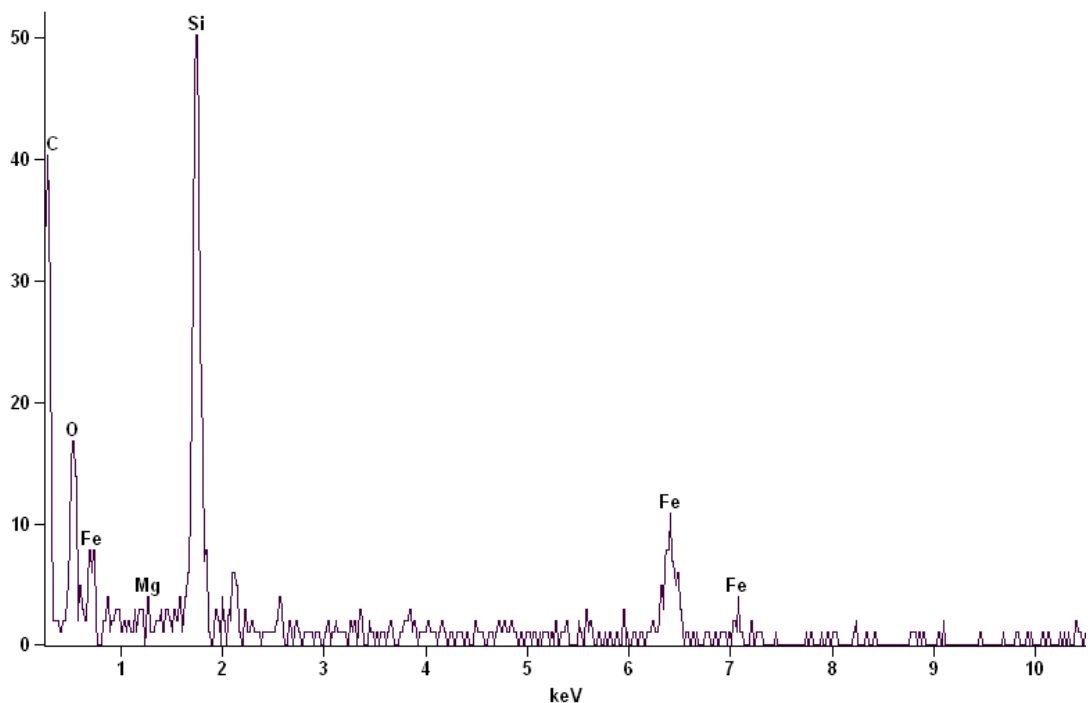
Graph showing the approximate content in the mixture after liquid sintering

Element Line	Net Counts	Int. Cps/nA	Weight %	Weight % Error	Atom %	Atom % Error	Formula	Standard Name
C K	205	0.000	2.46	+/- 2.20	51.02	+/- 3.98	C	
O K	87	0.000	1.65	+/- 1.29	16.89	+/- 1.75	O	
Mg K	0	0.000	0.00	---	0.00	+/- 0.00	Mg	
Si K	421	0.000	26.04	+/- 0.95	18.16	+/- 0.73	Si	
Si L	0	0.000	---	---	---	---		
Fe K	113	0.000	69.83	+/- 6.66	13.93	+/- 2.59	Fe	
Fe L	52	0.000	---	---	---	---		
Total			100.00		100.00			

Table 7.6 : Quantitative Results for liquid sintered sample

7.8 X-Ray diffraction (XRD) :

XRD machine works on the principle of Bragg's law. English physicists Sir W.H. Bragg and his son Sir W.L. Bragg developed a relationship in 1913 to explain why the cleavage faces of crystals appear to reflect X-ray beams at certain angles of incidence (theta). The variable d is the distance between atomic layers in a crystal, and the variable lambda l is the wavelength of the incident X-ray beam; n is an integer. This observation was direct evidence for the periodic atomic structure of crystals postulated for several centuries.

$$n.\lambda = 2d \, Sin \, \theta$$
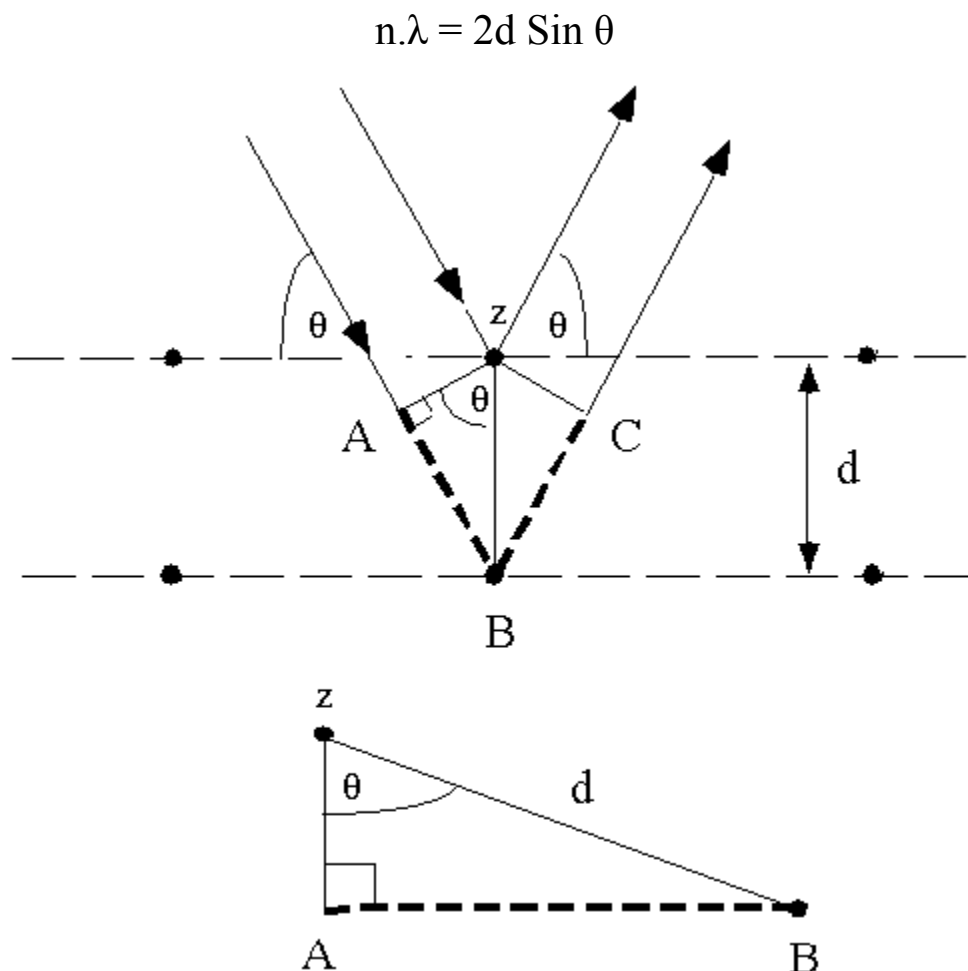
Fig 7.19 : Basic principle of reflection of the x-rays in XRD
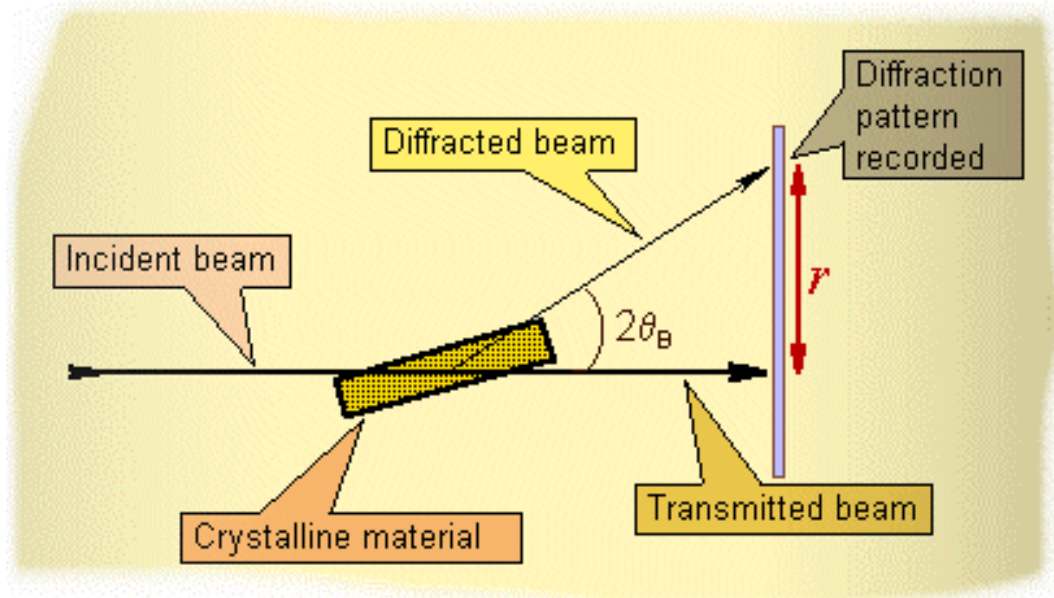
Fig 7.20 : Schematic representation of the material changes the direction of x-rays

Fig 7.21 : XRD machine set up at IIT roorkee

UnBonded

UnBonded - File: UnBonded.raw - Type: 2Th/Th locked - Start: 5.000 ° - End: 119.992 ° - Step: 0.019 ° - Step time: 38.4 s - Temp.: 25 °C (Room) - Time Started: 13 s - 2-Theta: 5.000 ° - Theta: 2.500 ° - C
Operations: Smooth 0.150 | Y Scale Mul 0.750 | Import
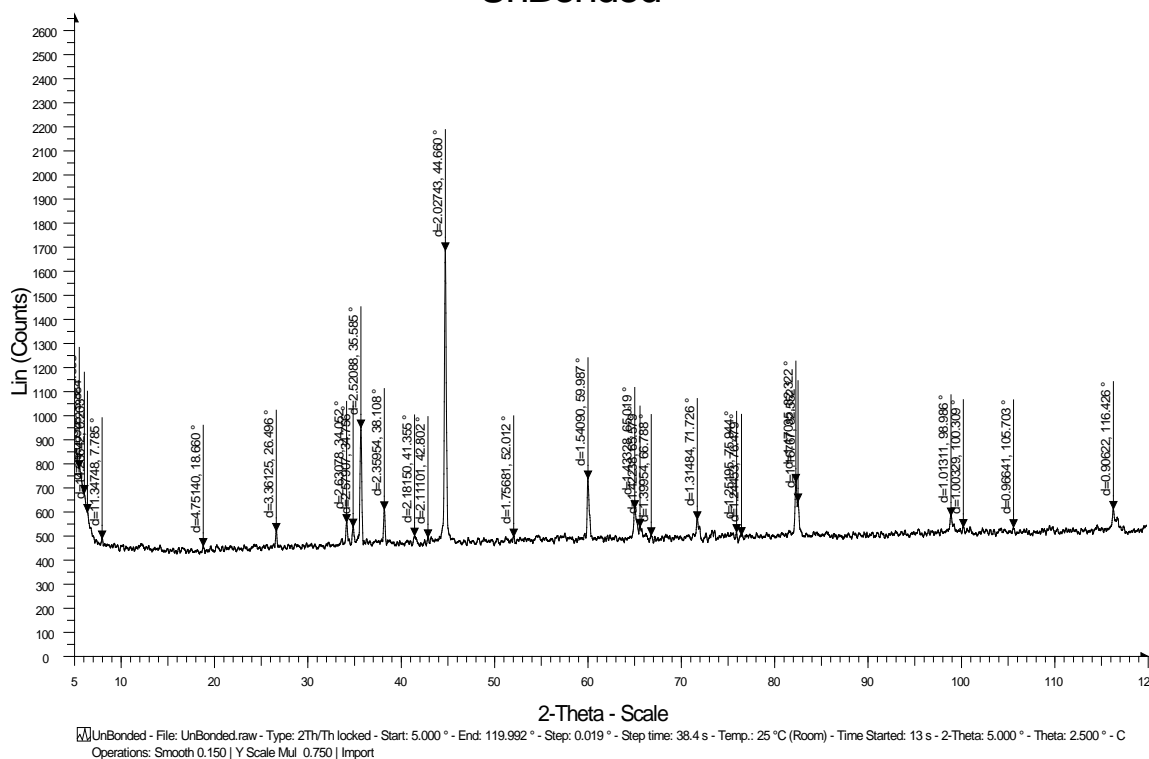
Unbonded mixture analysis on XRD

Peak No.	Angle (2θ)	3 x (Sin²θ/ Sin²θmin)	h² + k² + l²	[h k l]
1	26.496	3.000013998	3	[1 1 1]
2	34.052	4.89756487	5	[2 1 0]
3	38.108	6.088061204	6	[2 1 1]
4	44.66	8.246176588	8	[2 2 0]
5	52.012	10.98226038	11	[3 1 1]
6	59.987	14.27547798	14	[3 2 1]
7	65.019	16.49986589	16	[4 0 0]
8	66.788	17.30484212	17	[4 1 0]
9	71.726	19.60617739	20	[4 2 0]
10	75.944	21.62527948	21	[4 2 1]

Table 7.7 : [h k l] values corresponding to peak angles for unbonded mixture sample

6(2)

6(2) - File: 6(2).raw - Type: 2Th/Th locked - Start: 5.000 ° - End: 119.992 ° - Step: 0.019 ° - Step time: 38.4 s - Temp.: 25 °C (Room) - Time Started: 11 s - 2-Theta: 5.000 ° - Theta: 2.500 ° - Chi: 0.00 ° - Ph
Operations: Smooth 0.150 | Y Scale Mul 0.750 | Import
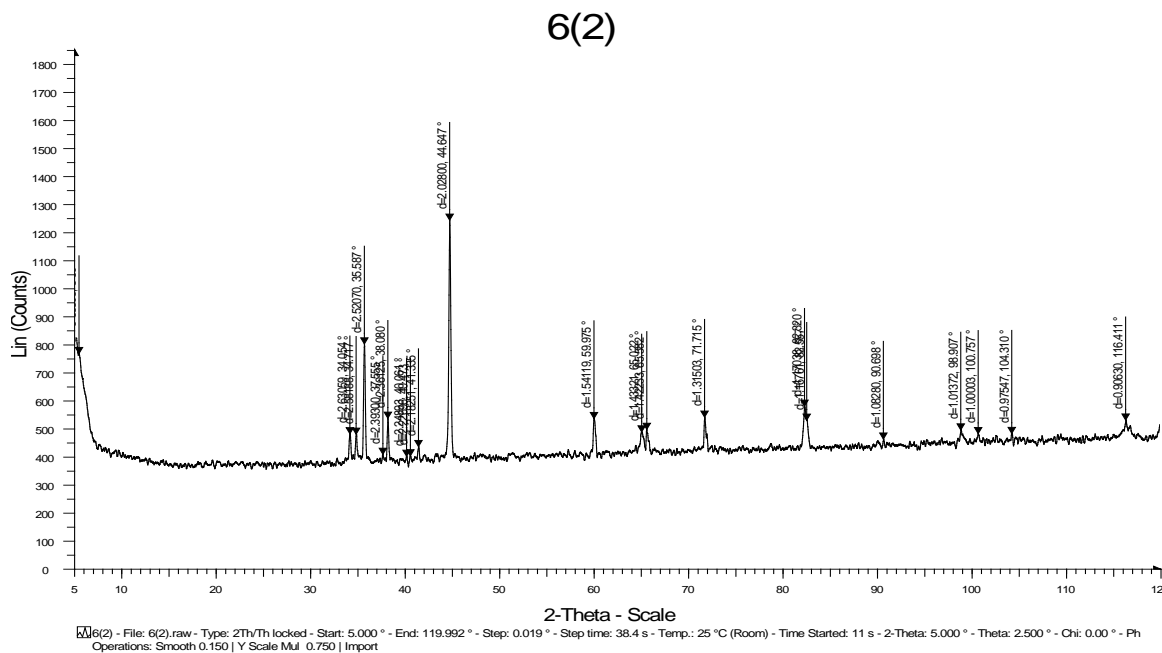
Solid sintered powder analysis on XRD

Peak No.	Angle (2θ)	3 x (Sin²θ/ Sin²θmin)	h² + k² + l²	[h k l]
1	34.054	3.000171842	3	[1 1 1]
2	37.555	3.625461759	4	[2 0 0]
3	40.473	4.186285403	4	[2 0 0]
4	44.647	5.048113593	5	[2 1 0]
5	59.975	8.740765793	9	[3 0 0]
6	65.022	10.10723874	10	[3 1 0]
7	71.715	12.86730213	13	[3 2 0]
8	82.32	14.81125612	14	[3 2 1]
9	90.698	17.70787433	17	[3 2 2]

Table 7.8: [h k l] values corresponding to peak angles for solid sintered samples

4 - File: 4.raw - Type: 2Th/Th locked - Start: 5.000 ° - End: 119.992 ° - Step: 0.019 ° - Step time: 38.4 s - Temp.: 25 °C (Room) - Time Started: 13 s - 2-Theta: 5.000 ° - Theta: 2.500 ° - Chi: 0.00 ° - Phi: 0.0
Operations: Smooth 0.150 | Y Scale Mul 0.750 | Import
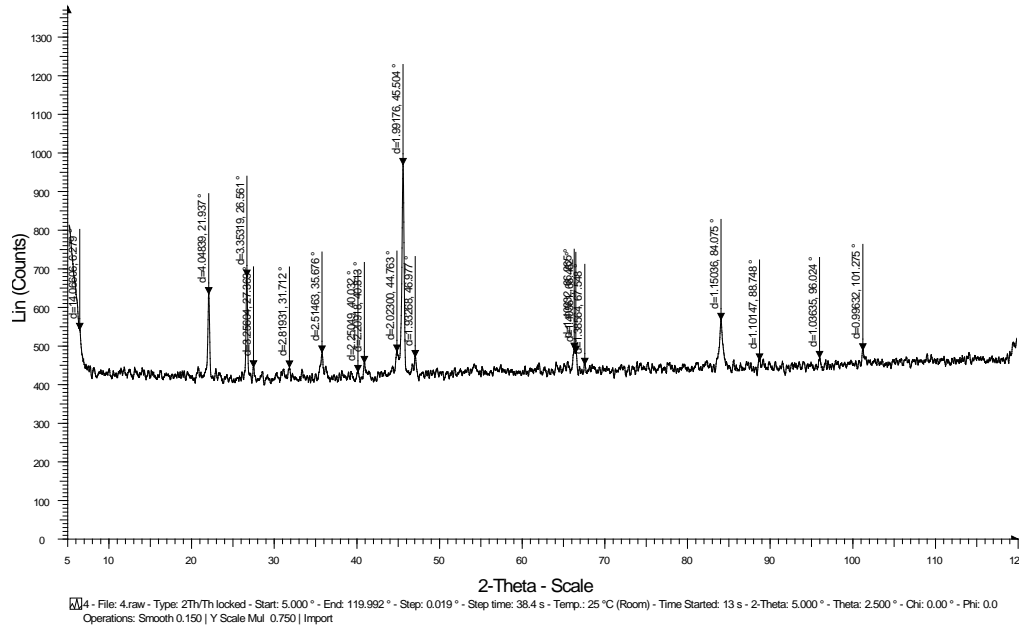
Liquid sintered powder analysis on XRD

Peak No.	Angle (2θ)	3 x (Sin²θ / Sin²θmin)	h² + k² + l²	[h k l]
1	21.937	3.000000023	3	[1 1 1]
2	26.561	4.372963583	4	[2 0 0]
3	27.369	4.637914058	4	[2 0 0]
4	31.712	6.186010686	6	[2 1 1]
5	35.676	7.775952733	8	[2 2 0]
6	40.032	9.708527489	10	[3 1 0]
7	40.813	10.07474118	10	[3 1 0]
8	44.763	12.0147157	12	[2 2 2]
9	45.504	12.39450348	13	[3 2 0]
10	46.977	13.16382725	13	[3 2 0]
11	66.265	24.75635257	24	[4 2 2]
12	66.462	24.88686254	24	[4 2 2]

Table 7.9: [h k l] values corresponding to peak angles for liquid sintered sample

7.9 Vibration Sample Magnetometer (VSM Testing) :

The magnetic properties of solids are very important, and attempts to understand them have led to a deep insight into the fundamental structure of many solids, both metallic and non-metallic. The VSM is the instrument used to measure the magnetic moment, the most fundamental quantity in magnetism, of solid samples.

When a sample material is placed in uniform magnetic field, a dipole moment proportional to the product of sample susceptibility and applied field is induced in the sample. If the sample is made to undergo sinusoidal motion as well, an electrical signal will be induced in suitable located stationary pick-coils. This signal, which is at the vibration frequency, is proportional to the magnetic moment, vibration amplitude and vibration frequency. The instrument displays the magnetic moment in e.m.u. units.

7.11.1 Specifications:

1. **Range:** 0.00001 to 10000 e.m.u.
2. **Magnetic field :** -10 to +10 kOe
3. **Temperature range :** 77 to 1050 K
4. **Sample weight :** Powder 20mg
5. **Rotation :** up to 360° w.r.t magnetic field
6. **Recording :** X-Y/(t) Recorder
7. **Sample size :** Diameter 2.5mm, Length 1-2.5mm

Fig 7.22 : VSM set-up at IIT Roorkee

Sample Code   = sem1 (Unbonded mixture)

Weight of the Sample = 0.06123 Grams

Max Current   = 30 Amp.

Reading No.   = 150

Scan Time   = 900 Seconds

VSM Range   = 10

Gauss Meter Range   = 10

Lab Temperature   = 28.2 C

Magnetic Field (gauss)	Total Magnetic Moment (emu)	Magnetic Moment of holder	Net magnetic moment of sample	Net moment / weight of sample (emu/g)
315	0.478	0.002349	0.475651	7.671790323
729	1.889	0.002677	1.886323	30.42456452
2069	4.905	0.003473	4.901527	79.0568871
3098	6.426	0.003821	6.422179	103.5835323
4014	7.33	0.004059	7.325941	118.1603387
5126	8.025	0.004267	8.020733	129.3666613
6121	8.443	0.004451	8.438549	136.105629
7161	8.7	0.004787	8.695213	140.245371
9198	8.976	0.005133	8.970867	144.6914032
9614	9.018	0.004464	9.013536	145.3796129
8594	8.94	0.004402	8.935598	144.1225484
7029	8.741	0.004637	8.736363	140.9090806
5340	8.307	0.004443	8.302557	133.9122097
4018	7.628	0.003988	7.624012	122.9679355
3091	6.887	0.003819	6.883181	111.0190484
1849	5.242	0.00379	5.23821	84.48725806
926	3.476	0.003199	3.472801	56.01291935

514	2.431	0.002957	2.428043	39.16198387
1	0.99	0.002416	0.987584	15.92877419
-826	-1.812	0.001193	-1.813193	-29.24504839
-1238	-2.949	0.000726	-2.949726	-47.57622581
-1746	-3.992	0.000439	-3.992439	-64.39417742
-2572	-4.557	0.000064	-4.557064	-73.50103226
-3497	-5.695	-0.000052	-5.694948	-91.854
-4718	-6.774	-0.000651	-6.773349	-109.2475645
-6892	-7.626	-0.000746	-7.625254	-122.9879677
-9045	-8.772	-0.001119	-8.770881	-141.4658226
-10315	-8.783	-0.001273	-8.781727	-141.6407581
-9055	-8.704	-0.001137	-8.702863	-140.3687581
-7624	-8.699	-0.001286	-8.697714	-140.2857097
-5638	-8.196	-0.000682	-8.195318	-132.1825484
-3912	-7.693	-0.000395	-7.692605	-124.0742742
-2159	-6.984	-0.000155	-6.983845	-112.6426613
-816	-5.266	0.000379	-5.266379	-84.94159677
-403	-4.176	0.000737	-4.176737	-67.36672581
7	-2.894	0.001214	-2.895214	-46.697
511	-1.066	0.001909	-1.067909	-17.22433871
929	0.12	0.002606	0.117394	1.893451613
1341	1.524	0.003029	1.520971	24.53179032
2263	3.992	0.003379	3.988621	64.33259677
3087	5.232	0.003632	5.228368	84.32851613
4411	6.923	0.00382	6.91918	111.5996774
6511	7.95	0.00365	7.94635	128.1669355
9610	9.002	0.004267	8.997733	145.1247258

Table 7.10 : VSM results for un-sintered sample

Hysteresis loop curve for unbonded mixture

Sample Code   = SEM6 (Solid sintered)

Weight of the Sample = 0.07111 Grams

Max Current   = 30 Amp.

Reading No.   = 150
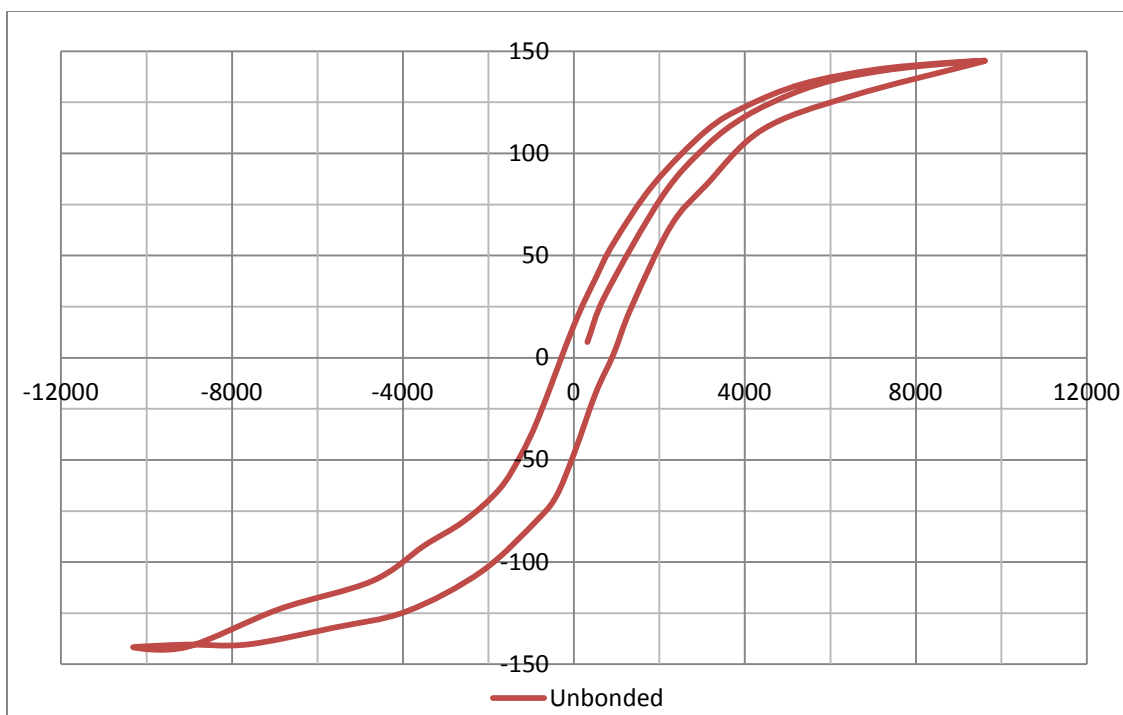
Scan Time   = 900 Seconds

VSM Range   = 10

Gauss Meter Range   = 10

Lab Temperature   = 29.2 C
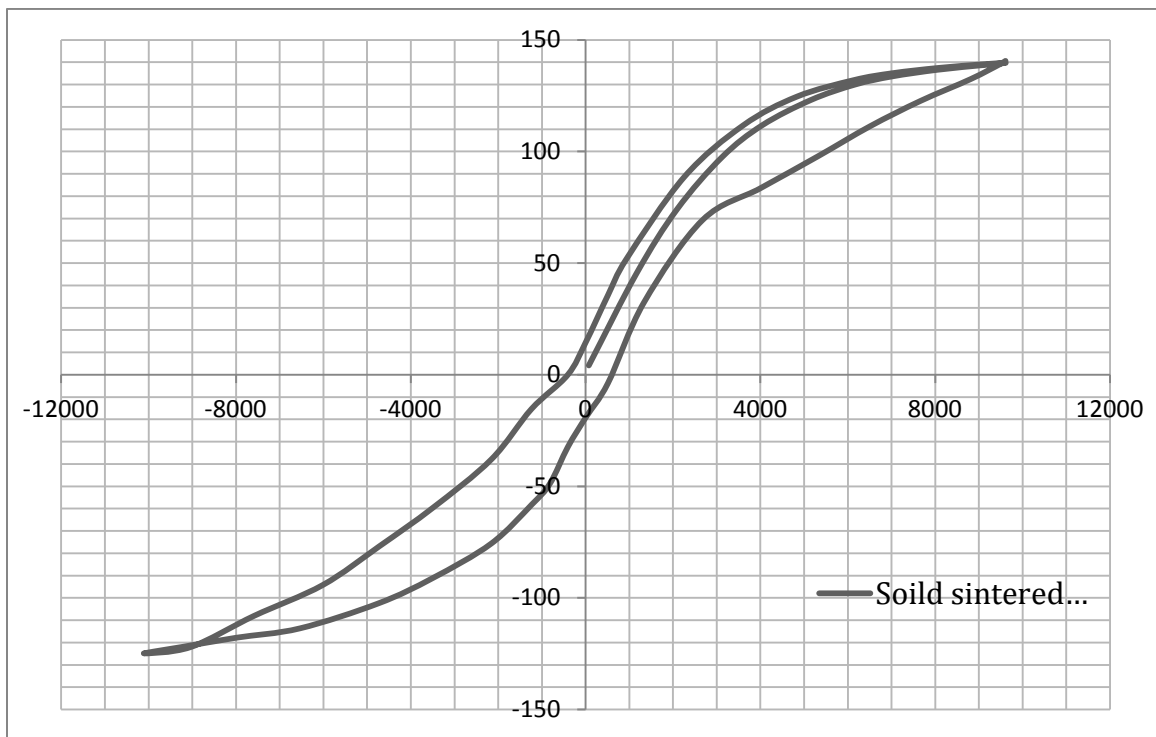
Magnetic Field (gauss)	Total Magnetic Moment (emu)	Magnetic Moment of empty Holder	Net magnetic moment of sample	Net moment/ wt. of sample (emu/g)
73	0.299	0.00325	0.29575	4.159634318
1170	3.247	0.00687	3.24013	45.57144866
2091	5.277	0.00886	5.26814	74.09479606
3120	6.941	0.01145	6.92955	97.46202532

4040	7.958	0.01201	7.94599	111.7579466
5156	8.765	0.01306	8.75194	123.0933896
7008	9.516	0.01405	9.50195	133.6420534
8052	9.728	0.01412	9.71388	136.6227848
9613	9.948	0.01517	9.93283	139.7022504
9085	9.904	0.01546	9.88854	139.0793249
8068	9.788	0.01546	9.77254	137.44782
7025	9.62	0.01442	9.60558	135.0995781
6140	9.399	0.01309	9.38591	132.0099859
4834	8.871	0.01244	8.85856	124.5929677
3604	7.953	0.0107	7.9423	111.7060478
2260	6.313	0.00835	6.30465	88.67299578
926	3.676	0.00686	3.66914	51.60534459
513	2.545	0.0057	2.5393	35.71448664
0	1.029	0.0035	1.0255	14.4233474
-411	-0.006	0.00138	-0.00738	-0.103797468
-1239	-1.093	-0.00167	-1.09133	-15.34922644
-2159	-2.703	-0.00388	-2.69912	-37.96230661
-3496	-4.245	-0.00551	-4.23949	-59.62714487
-4719	-5.471	-0.00731	-5.46369	-76.84514768
-6013	-6.706	-0.00817	-6.69783	-94.20295359
-7584	-7.689	-0.00926	-7.67974	-108.0132208
-9041	-8.687	-0.01003	-8.67697	-122.0389592
-10111	-8.887	-0.01058	-8.87642	-124.8441632
-9257	-8.687	-0.01016	-8.67684	-122.0371308
-8001	-8.387	-0.00794	-8.37906	-117.8489451
-6535	-8.086	-0.00689	-8.07911	-113.6302391
-4733	-7.286	-0.00703	-7.27897	-102.376512
-3501	-6.486	-0.00627	-6.47973	-91.13544304

-2160	-5.384	-0.00464	-5.37936	-75.65907173
-817	-3.472	-0.00272	-3.46928	-48.79437412
-405	-2.298	-0.00195	-2.29605	-32.29324895
7	-1.353	-0.00036	-1.35264	-19.02447257
510	-0.27	0.00212	-0.27212	-3.827285513
1339	2.317	0.00502	2.31198	32.51729958
2674	4.933	0.00733	4.92567	69.27805907
4001	5.95	0.00846	5.94154	83.56596343
5316	6.968	0.00966	6.95834	97.86694796
6509	7.926	0.01077	7.91523	111.3253165
7658	8.73	0.01088	8.71912	122.6317862
8808	9.426	0.01059	9.41541	132.4248945
9487	9.909	0.0119	9.8971	139.1997187
9608	10.01	0.01261	9.99739	140.6102672

Table 7.11: VSM results for solid sintered sample

Hysteresis loop for solid sintered powder

Sample Code = sem4 (Liquid sintered)

Weight of the Sample = 0.02686 Grams

Max Current = 30 Amp.

Reading No. = 150

Scan Time = 900 Seconds

VSM Range = 10

Gauss Meter Range = 10

Lab Temperature = 29.2 C

Mag. Field (gauss)	Total Mag. Moment (emu)	Mag. Moment of empty holder	Net magnetic Moment	Net moment/ wt of sample (emu/g)
75	0.162	0.002122	0.159878	7.9939
567	0.546	0.002264	0.543736	27.1868
1171	1.033	0.00251	1.03049	51.5245
2092	1.425	0.00248	1.42252	71.126
4653	1.737	0.002487	1.734513	86.72565
7007	1.798	0.002456	1.795544	89.7772
9604	1.824	0.00243	1.82157	91.0785
7023	1.802	0.002579	1.799421	89.97105
3090	1.666	0.002469	1.663531	83.17655
1339	1.316	0.002667	1.313333	65.66665
514	0.829	0.002543	0.826457	41.32285
1	0.34	0.002107	0.337893	16.89465
-411	-0.205	0.001843	-0.206843	-10.34215
-826	-0.659	0.001701	-0.660701	-33.03505
-1239	-0.992	0.001519	-0.993519	-49.67595
-1747	-1.249	0.001416	-1.250416	-62.5208
-2571	-1.536	0.001476	-1.537476	-76.8738
-5611	-1.791	0.001393	-1.792393	-89.61965
-10260	-1.857	0.000951	-1.857951	-92.89755

-6038	-1.821	0.001206	-1.822206	-91.1103
-2984	-1.689	0.001322	-1.690322	-84.5161
-1746	-1.475	0.001225	-1.476225	-73.81125
-815	-1.084	0.001294	-1.085294	-54.2647
-402	-0.776	0.001418	-0.777418	-38.8709
7	-0.337	0.00159	-0.33859	-16.9295
512	0.237	0.001988	0.235012	11.7506
929	0.703	0.002322	0.700678	35.0339
1340	1.023	0.00226	1.02074	51.037
1849	1.263	0.002199	1.260801	63.04005
2674	1.529	0.002728	1.526272	76.3136
4002	1.69	0.002549	1.687451	84.37255
7655	1.803	0.002727	1.800273	90.01365
9600	1.822	0.002901	1.819099	90.95495

Table 7.12 : VSM results for liquid sintered sample
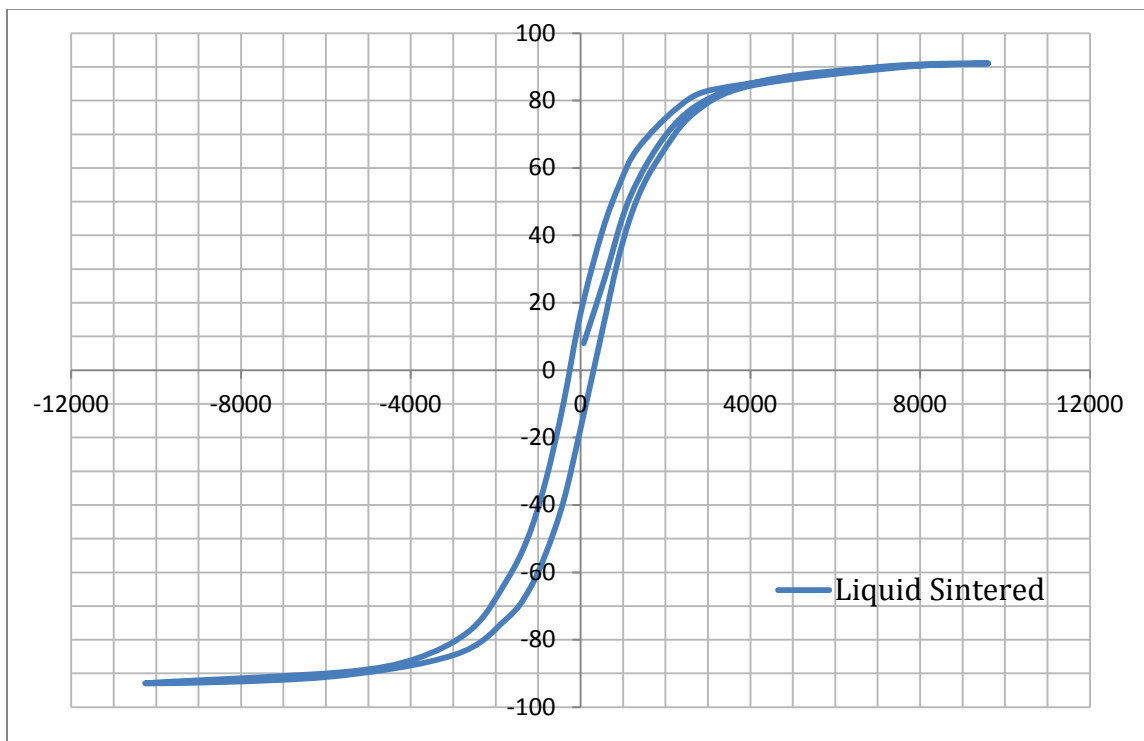
Hysteresis curve for liquid sintered powder

8.1 Discussion on results & graphs:

1. **Compressive strength** – It has been found that the compressive strength of the solid & liquid sintered sample increases in the parabolic and linear manner respectively as the compaction pressure increases because as the pressure increases the powder particles come closer to one another and thus formed strong mechanical bond. On the other hand, the compressive strength also increases with increasing the sintering temperature because more diffusion occurs at high temperature and consequently reduces the dislocations.

2. **Density –** The graph of density vs compaction load shows that density increases with increase in the compaction pressure as the intermolecular spacing reduces and mechanical bonding improves. The density also increases with sintering temperature because at high temperature the diffusion of particles and liquid shrinkage phenomenon occurs which decreases the interatomic spacing. It has been found that the green samples have low density as compared to sintered sample.

3. **Micro-hardness –** It has been observed that micro-hardness increases with increase in the compaction pressure due to increase in the grain size. The increase in the grain size offers more resistance to move the dislocations. Also the micro-hardness increases with increase in the sintering temperature. Higher the sintering temperature, higher will be the tendency of the material to achieve crystalline structure from the amorphous.

4. **Microstructure –** The micrograph study has been shown that the iron particles completely mix with the silicon carbide particles homogeneously and the silicon carbide phase have 29 percent area where as iron phase have around 71 percent area. The micrographs of etched iron‑SiC specimen was revealing grains at the SiC‑iron interface.

5. **SEM analysis –** The SEM image in Fig. 7.9 and 7.10 shows the morphology of silicon carbide and carbonyl iron powders respectively. Iron powder has a spherical

shape and silicon carbide has irregular shape. The composition of silicon carbide powder as given by the powder supplier contains manganese, sulphur and phosphorus and nickel of 0.120, 0.021, 0.016 and 0.016% and the rest silicon carbide. The grain size of iron measured by particle size counter equipment varied from 6 to 15 micron with an average grain size of 10 microns. The grain size of silicon carbide varied from 30 to 40 micron with an average grain size of 37 microns. Fig. 7.11 shows the morphology of silicon carbide- iron composite particles before sintering and fig. 7.12 to 7.17 shows the material after sintering at different compaction pressure and different sintering cycle. It is clearly seen from Fig. 7.14 and 7.16 that there is a uniform sintering of the particles.

6. **Energy Dispersive Spectroscopy (EDS)** – The EDS results clearly shown that the composition of the two component were basically exists. The iron and the oxides of iron phase have around 69 to 70 percent by weight and the silicon phase have around 26 percent by weight. The remaining constituents are carbon and oxygen with around 2 and 1.5 percent respectively. The study of EDS graph shows that the percentage of oxygen in the material increases very slightly due to some unwanted oxidation.

7. **X-RAY Diffraction** – The XRD graph clearly shows that the highest peak for unsintered powder comes at 44.66 degrees of 2θ angle for Fe_2O_3. The miller indices of that phase is supposed to be [2 2 0] and the crystal structure is simple cubic. Rest of the peaks have variation of 2θ in the range of 20 to 120 degree and different phases present in the material are of Fe_3O_4, SiC and Fe. Now the sintered sample at 1000 degree have been examined. It is clearly shown by the graph that the highest peak comes at 44.64 degree for Fe_3O_4 and is having FCC crystal structure with miller indices of [2 1 0] . The phases present in the sample are iron oxide, silicon carbide, pure iron and silicon. The liquid sintering at 1545 degree diffuses the iron particle within the material and a phase of FeO exixts. The crystal structure of FeO is hexagonal and the peak for this material is 40.83 degree. The miller indices is [3 1 0]. The highest peak comes at 45.8 degree for silicon carbide phase. The crystal structure is hexagonal and the miller indices for this phase is [3 2 0].

8. **VSM analysis –** The study of magnetic moment clearly shows that magnetic properties decreases with the increase in the sintering temperature. The unsintered powder have maximum magnetic moment of 145 emu/g at 0.961 tesla. The solid sintered sample have maximum mag. Moment of 139.7 emu/g at 0.9613 tesla. The maximum value decreases very slightly and the materail didn't loose magnetic properties. The liquid sintered sample shows the max. value of 01.08 emu/g at 0.9604 tesla. So the study clearly shows that the temperature alters the material's magnetic properties and material shows paramagnetic behaviour instead of ferromagnetic.

8.2 Conclusion: The present study on the powder processing, density, microstructure, micro hardness, SEM, XRD, VSM, and mechanical properties of SiC- CIP composite were undertaken to study the following:

1. The silicon carbide and CIP based sintered magnetic abrasive powders were prepared by powder metallurgy method.

2. The mechanical properties such as compressive strength, density, micro-hardness of the green and sintered pellets have been studied using the universal testing machine, archimidies principle, and vickers hardness tester.

3. It has been found that the micro-hardness increases with sintering temperature and also with compaction pressure. The rate of increase of this mechanical property is linear for temperature upto 2000 ˚C and then become constant beyond 2000 ˚C.

4. The density varies with the compaction pressure. When the compaction pressure is higher, the mechanical bonds becomes stronger and the porosity within the material decreases so density of the material increases. The value of density of the liquid sintered sample is slightly higher than the solid sintered. This can be attributed to the fact that at higher sintering temp., the extent of melting is higher as the heat energy absorbed by the powder is more. This results in improved melting which contributes to the higher density. These observations are in line with other researchers (Simchi et al., 2001; Simchi and Pohl, 2003).

5. Characterization of the sintered magnetic abrasive has been studied by SEM, EDS, XRD and VSM to study the morphology, chemical composition, crystallography and magnetic properties. It has been found that the particle size of the powder ranges between 10 to 53 microns with average particle size of 37 microns. The materials present in the mixture with less than 0.01 percent by weight are phosphorous, nickel, chromium, molybdenum and copper. The phases present in the powder were SiC, Fe_2O_3 , Fe, Fe_3O_4 with miller indices of [1 0 4], [1 1 6], [2 0 0], [3 1 1] respectively. The magnetic properties such as magnetic moment decreases with increasing the sintering temperature.

8.3 Future Scope:

The present study reveals that powder processing is an important step for achieving a dense microstructure. The magnetic abrasive will be used for finishing purpose in magnetic abrasive finishing, magnetorheological finishing and rotational magnetic abrasive finishing. Also improve the result of density and magnetic property of SiC and CIP composites by inert gas sintering and compaction load. The magnetic abrasive will be used in aerospace and electronics industries for finishing of hard material which is not easy to finish by conventional method.

REFERENCES

1. Biswas,K. et al. (2001)."Liquid phase sintering and microstructure–property relationships of silicon carbide ceramics with oxynitride additives.", Materials Chemistry and Physics, 67 (2001), 180–191.

2. Borgstrom, H. and Nyborg, L. (2007)."Liquid phase sintering of ferrous powder metallurgical materials." Journal of iron and steel research,international,14(5),70-76.

3. Borsa, C. E. et al. (1998). "Liquid phase sintering of Al_2O_3/SiC nano composites.", Journal of the European Ceramic Society ,19 (1999), 615-621.

4. Ermer, E.B. et al. (2001). "Influence of sintering activators on structure of silicon carbide." Solid State Ionics (141–142) , 523–528.

5. Gomez, E. et al. (2003). "Liquid phase sintering of SiC with additions of Y_2O_3, Al_2O_3 and SiO_2" Journal of the European Ceramic Society,24 (2004), 2895–2903.

6. Li, G. et al. (1997). "Liquid Phase Sintering of Metal Matrix Composites.", Journal of Materials Processing Teclmology, 63 (1997), 286-291.

7. Magnani, G. et al. (2004)."Properties of liquid phase pressureless sintered silicon carbide obtained without sintering bed.", Journal of the European Ceramic Society 25 (2005) ,1619–1627.

8. Olevsky, E. A. (1997). "Theory of sintering: from discrete to continuum." Materials Science and Engineering, R23 (1998), 41–100.

9. Rahimian, M. et al. (2009). "The effect of particle size, sintering temperature and sintering time on the properties of Al–Al2O3 composites, made by powder metallurgy.", Journal of Materials Processing Technology 209 (2009), 5387–5393.

10. Rodriguez, M.C. et al. (2005). "Effect of atmosphere and sintering time on the microstructure and mechanical properties at high temperatures of α-SiC sintered with liquid phase Y_2O_3–Al_2O_3." Journal of the European Ceramic Society, 26 (2006), 2397–2405.

11. She, J.H. and Ueno, K. (1999). "Effect of additive content on liquid-phase sintering on silicon carbide ceramics." Materials research bulletin, 34(10/11), 1629–1636.

12. Upadhyaya, A. and Upadhyaya, G. S. (2011). "Powder metallurgy." Universities press private limited , Himayatnagar ,Hydrabad 500029(A.P.)India,79-368.

13. Van dijen, F. K. and Mayer, E. (1995). "Liquid Phase Sintering of Silicon Carbide." Journal of the European Ceramic Society, 16 (1996), 413-420.

14. C.S. Ramesha, C.K. Srinivas, (2008). "Friction and wear behavior of laser-sintered iron–silicon carbide composites", Journal of Materials Processing Technology 209 (2009) 5429–5436.

15. S. Hayuna, V.Parisb, R.Mitrania, S.Kalabukhova, M.P.Dariela, E.Zaretskyb, N.Frage (2012), "Microstructure and mechanical properties of silicon carbide processed by Spark Plasma Sintering (SPS)", Ceramics International 38 (2012) 6335–6340.